京都大学学術情報リポジトリ
KURENAI 紅
Kyoto University Research Information Repository

京都大学
KYOTO UNIVERSITY

Title	Synergistic roles of the proteasome and autophagy for mitochondrial maintenance and chronological lifespan in fission yeast.
Author(s)	Takeda, Kojiro; Yoshida, Tomoko; Kikuchi, Sakura; Nagao, Koji; Kokubu, Aya; Pluskal, Tomás; Villar-Briones, Alejandro; Nakamura, Takahiro; Yanagida, Mitsuhiro
Citation	Proceedings of the National Academy of Sciences of the United States of America (2010), 107(8): 3540-3545
Issue Date	2010-02-23
URL	http://hdl.handle.net/2433/139449
Right	©2010 by the National Academy of Sciences
Type	Journal Article
Textversion	author

Kyoto University

Title

Synergistic Roles of the Proteasome and Autophagy for Mitochondrial Maintenance and Chronological Life Span in Fission Yeast

Kojiro Takeda[a], Tomoko Yoshida[b], Sakura Kikuchi[a], Koji Nagao[a], Aya Kokubu[a], Tomáš Pluskal[a], Alejandro Villar-Briones[a], Takahiro Nakamura[c], and Mitsuhiro Yanagida[a, c, 1]

[a]G0 Cell Unit, [b]Electron Microscope Room, Okinawa Institute of Science and Technology (OIST), 12-22 Suzaki, Uruma, Okinawa 904-2234, Japan

[c]Core Research for Evolutional Science and Technology Research Program, Japan Science and Technology Corporation, Graduate School of Biostudies, Kyoto University, Sakyo-ku, Kyoto 606-8501, Japan

Classification: Biological Sciences, Cell Biology

Manuscript Information: nineteen pages and 4 figures (10 SI)

Abbreviations: ROS (Reactive Oxygen Species), VEG (Vegetative proliferation)

[1]To whom correspondence should be addressed;
Mitsuhiro Yanagida
yanagida@kozo.lif.kyoto-u.ac.jp,
Phone: +81-75-753-4205
Fax: +81-75-753-4208

Abstract

Regulations of proliferation and quiescence in response to nutritional cue are important for medicine and basic biology. The fission yeast *Schizosaccharomyces pombe* serves as a model, owing to the shift of proliferating cells to the metabolically active quiescence (designate G0-phase hereafter) by responding to low nitrogen source. *S. pombe* G0-phase cells keep alive for months without growth and division. Nitrogen replenishment reinstates vegetative proliferation phase (designate VEG). Some forty genes required for G0 maintenance were identified, but there still remain many to be identified. We here show using mutants that the proteasome is required for maintaining G0 quiescence. Functional outcomes of proteasome in G0 and VEG-phases appear to be quite distinct. Upon proteasome dysfunction, a number of anti-oxidant proteins and compounds responsive to ROS (reactive oxygen species) are produced. In addition, autophagy-mediated destruction of mitochondria occurs, which suppresses the loss of viability by eliminating ROS-generating mitochondria. These defensive responses are found in G0 but not in VEG, suggesting that the main function of proteasome in G0-phase homeostasis is to minimize ROS. Proteasome and autophagy are thus collaborative to support life span of *S. pombe* G0-phase.

Introduction

¥body

The transition between cell proliferation and G0/quiescent phase is finely controlled in response to extracellular conditions, such as growth factors and nutrient availability(1-3). The regulation of entry and exit to/from G0 phase is strongly relevant to tumorigenesis and tissue regeneration. Failure to maintain terminally differentiated cells in the healthy G0 phase may also lead to diseases such as neurodegeneration. Therefore, regulations of G0 entry, exit and maintenance are medically important topics.

The fission yeast *Schizosaccharomyces pombe* has been adopted as an excellent model organism for cell cycle research and cell biology, owing to its genetic tractability and similarity to higher eukaryotic cells. Like mammalian cultured cells, which are introduced to G0 phase by serum starvation(1), proliferating cells of the fission yeast enter G0 phase in response to low nitrogen(4-6). Following nitrogen withdrawal from the medium, fission yeast cells immediately cease cell growth, perform division twice and arrest in G0 phase (G0 entry). Arrested G0 cells are metabolically active, viable for more than one month (G0 maintenance) and reinstate proliferation by nitrogen replenishment (G0 exit). We take advantage of this feature of fission yeast and adopt this yeast as a model organism to study the regulatory mechanisms of G0 phase. Previously, we identified 7 genes required for G0 entry and 36 genes for maintenance(5, 6), including regulators of transcription, chromatin dynamics, vesicle transport, and the actin cytoskeleton. However, many other factors may remain unidentified.

The ubiquitin/proteasome system, a major proteolytic mechanism in the cell(7), is one possible candidate pathway that may be essential for G0 phase. The ubiquitin/proteasome system is involved in cellular essential pathways, such as cell cycle control and protein quality control. The proteasome is required for M phase progression(8), because the proteasome is responsible for the degradation of the mitotic regulators, Cyclin B and Securin(9-13). In fission yeast, the proteasome is localized to the nucleus, which guarantees the rapid degradation of Cdc13/Cyclin B and Cut2/Securin in the nucleus(14-16). In G0 phase, however, the essential roles of the proteasome have not been understood well so far. In this study, we attempt to elucidate essential proteasomal functions specific to G0 phase. We found the proteasome complex is exported from the nucleus to the cytoplasm upon G0 entry. Inactivation of the proteasome in G0 phase is lethal and leads to the accumulation of cellular reactive oxygen species (ROS) and massive degradation of mitochondria by autophagy (mitophagy), which inhibits further accumulation of ROS. We suggest that the proteasome and selective mitophagy cooperatively contribute to G0 maintenance via reducing lethal accumulation of ROS.

Results

Striking alteration of the 26S proteasome localization was observed during the shift from VEG to G0 phase of *S. pombe*. Green fluorescent protein (GFP) tagged to α4 (20S component) or Pad1 /Rpn11 (19S component) was chromosomally integrated under the native promoter and used to locate the 26S proteasome. In VEG, the proteasome is enriched in the nucleus and nuclear envelope(14-16). In G0, nuclear localization signals of α4- and Pad1-GFP were greatly diminished with the increase of cytoplasmic GFP-signals, while the signal on the nuclear periphery persisted (Fig. 1a and Fig. S1; G0 and VEG cells are, respectively, round- and rod-shaped). The signals were not intrinsic fluorescence, as cells without GFP-tagging showed no fluorescence (Fig. 1a). The proteasome signals remained in the nucleus for 6h after the removal of nitrogen (–N), when most cells had finished the second division and were competent to mate if cells with the opposite mating type existed. The nuclear proteasome was diminished at 12h at the timing of G0 entry(6) (Fig. 1b). The level of proteasome subunit was unchanged during VEG to G0 transition, while the level of Cdc13 mitotic cyclin greatly reduced(6) (Fig. 1c). The cytoplasmic α4-GFP signal returned to the nucleus following treatment with the Crm1/exportin inhibitor leptomycin B (LMB)(17) (Fig. 1d), indicating that the proteasome export to cytoplasm increased at the G0 shift.

To examine whether proteasome-mediated proteolysis existed in G0-phase, we first isolated the 26S proteasome from both VEG and G0 extracts and analyzed the compositions by mass spectrometry (Fig. S2). Reported subunits and accessory proteins of the 26S complex(18) were all present in both VEG and G0, indicating that the regular 26S proteasome existed in G0. Next, proteolysis and ubiquitination in G0 were examined using *mts3-1*(8), a temperature-sensitive mutant of the proteasome subunit Mts3/Rpn12. Cut8 (a proteasomal localization factor whose degradation in VEG depends on proteasomal activity(15, 16)) found to be short lived in G0 like in VEG phase (Fig. 1e). After the addition of cycloheximide, a protein synthesis inhibitor, the level of Cut8 was diminished within 15 min in both VEG and G0 phase in wild type (WT), but not in the *mts3-1*, suggesting that Cut8 was actively degraded in a proteasome-dependent manner at a similar rate in both VEG and G0. Indeed the level of poly-ubiquitinated proteins in G0 was already high in *mts3-1* at a permissive temperature (26°C), and further increased at the restrictive temperature (37°C) (Fig. 1f). These results established that 26S proteasome-mediated proteolysis was active in G0-phase.

The proteasome was essential for maintenance of the viability in G0. The *mts3-1* mutant decreased to 40% viability after 24h at 37°C, which further decreased to 0.1% after 72h at 37°C in G0 (Fig. 1g). WT sustained high viability (>80%) after 72 h at 37°C, and the

G0-arrested *mts3-1* cells did not lose viability at all for at least one week at 26°C (Fig. S1). The other proteasome mutant *pad1-932* also lost the viability in G0 at 37°C (Fig. S1)

Thin-section transmission electron microscopy (TEM) of WT and *mts3-1* (Fig. 1h-j) revealed abnormalities in cytoplasm and the nucleus in *mts3-1* at 37°C. First, mitochondria (indicated by m in WT at 37°C after 24h; Fig. 1h) were greatly diminished in *mts3-1*. Secondly, aberrant electron-dense materials (small arrow) and vesicle-like structures (arrowhead) formed in the mutant nucleus after 24h (Fig 1i) and the nuclear damages further progressed after 72h (Fig 1j). Nuclear chromatin structure stained by DAPI (inset) also became deformed. Unexpectedly, the intra-nuclear vesicle-like structures may be lipid-containing, as they were stained by Nile-Red that was used to reveal lipid droplets (storage particles) normally present in cytoplasm(19) (Fig. S3). A notable mutant phenotype at 26°C was that *mts3-1* divided only once and arrested after nitrogen withdrawal (Fig. 1k), while WT cells divided twice before arrest(6). The reason why the second division was omitted in *mts3-1* is unknown.

The decrease of mitochondria in G0 proteasome mutant cells 24h after the shift to 37°C was verified by Mitotracker Green stain(20) (Fig. S4). We then made GFP-tagged Sdh2 (succinate dehydrogenase subunit, a mitochondrial protein) integrated at the C-terminus of the chromosomal *sdh2*$^{+}$ gene. Resulting Sdh2-GFP signals expressed under the native promoter in WT and *mts3-1* mutant at 26°C behave like a mitochondria marker, whereas the GFP signal was greatly diminished in *mts3*-1 after 24h at 37°C (Fig. 2a and Fig, S4). The protein levels of Sdh2-GFP and Gcv1-FLAG (mitochondrial glycine decarboxylase, SPAC31G5.14) detected by immunoblot showed the time course decrease in *mts3-1* at 37°C after 12h (Fig. 2b). The decrease of mitochondrial protein Sdh2-GFP was observed in other proteasome mutants (*pad1-932*, *pts1-732* mutated in the β5 subunit, *ump1-346, -620* mutated in the 20S assembly factor(21); Fig. S4). In VEG phase, however, the Sdh2-GFP signal did not decrease at all after a temperature shift to 37°C, when the mutant ceased dividing completely and viability was reduced to 15% (Fig. 2c). Immunoblot (Fig. 2d) showed that Sdh2-GFP did not decrease in VEG even after 24h at 37°C (viability decreased to 0%). These results established that the marked degradation of mitochondria occurred specifically in G0 upon proteasomal inactivation.

To determine whether all of principal mitochondrial proteins disappeared in *mts3-1* mutant in G0, comprehensive proteomic analyses were performed, using liquid chromatography-tandem mass spectrometry(22) (LC-MS/MS; ThermoFisher LTQ). Proteins were extracted from WT and *mts3-1* cells at 37°C for 12h in G0 (control extracts made were from VEG cells cultured for 6h at 37°C). To compare abundance of individual proteins, the

scatter plots were used (Fig 2e-h). Location of each dot (inset) in the logarithmic X- and Y-axis indicates the protein abundance(22, 23) in the two extracts: when the levels of proteins between the two samples are identical or similar, the dots are distributed along the central diagonal line. In WT G0 cells, ~2,000 proteins were detected by LC-MS/MS, in which 256 (light blue dots) were mitochondrial proteins (a total of 696 mitochondria proteins among the 5,000 whole proteins reported in the Sanger Institute GeneDB). In two independently cultured WT G0 cell extracts (37°C, 12 h; Fig 2e), 97% of the 1917 detected proteins were located within the boundary of a 4-fold change in the two samples (indicated by two lines 4.0x and 0.25x). In contrast, 89% of 2043 proteins detected from WT and *mts3-1* G0 cells (37°C, 12h) were within a 4-fold change (Fig. 2f). The abundance of 125 proteins decreased to less than 0.25-fold in *mts3-1* (outside of upper diagonal line), and 60 of them (48%) were mitochondrial proteins (listed in the green columns of Table. S1). Three most greatly reduced (down to 1-5% in comparison with the levels in WT G0) proteins, Sdh2, Cyc1 (cytochrome c) and Ilv5 (acetohydroxyacid reductoisomerase) were mitochondrial proteins. These results showed that many, not all, of mitochondrial proteins reduced their levels in *mits3-1* G0 phase at 37°C. No particular type of mitochondrial proteins was specifically degraded. The experiment was replicated in VEG phase (Fig. 2g to h). As expected from cytological results, the proteomic decrease of mitochondrial proteins was insignificant.

The scatter plot of G0 proteomics data (Fig. 3a) revealed 110 proteins that showed a >4-fold increase in *mts3-1* versus WT at 37°C (Table. S2). Among them, the greatest increase (146-fold) was Hsp16 that belongs to the HSP20/alpha-crystallin heat shock protein family. Hsp16 increased not only by the temperature upshift, but also by cadmium, nutrient starvation, and DNA damage(24). Three others, SPAC11D3.01c (indicated by 1; similar to *N. crasssa* conidation protein 6), short chain dehydrogenases SPCC663.06c and SPCC663.08c (2 and 3, respectively) that prominently (>20-fold) increased in *mts3-1* are known to increase in the presence of H_2O_2(25) . SPAC83.17 (4), Multi protein bridging factor 1 [Mbf1] involved in transcriptional regulation of many process such as lipid metabolism(26), increased 33 fold in *mts3-1* and is responsive to both heat (>5-fold) and cadmium (~2.5-fold) like Hsp16. Indeed many (30%) of 110 proteins that increased >4-fold in *mts3-1* are responsive to H_2O_2 and/or cadmium stress (colored dots, see captions of Fig 3a). Proteasome dysfunction seems to activate a number of defensive functions directly (H_2O_2 responsive) and indirectly (cadmium responsive) against oxidative stresses(27).

To examine whether metabolic compounds against oxidative stress were produced in G0 *mts3-1*, metabolomic analysis was undertaken using LC/MS(28). Glutathione (GSH) and ergothioneine, both authentic anti-oxidant metabolites(29), were accumulated in

G0 *mts3-1* (>10-fold; Fig. 3b). Three duplicate experiments produced similar increase. GSH and ergothioneine also accumulated in different proteasome mutant, *pts1* -727 (Fig. S5).

H_2DCFDA, a chemical compound that produces fluorescence upon the reaction with ROS, was used to stain WT and *mts3-1* cells(30). As seen in Fig 3c, the fluorescent signals were strong in *mts3-1* G0 phase after 24h (viability = 36%), while WT G0 phase cells showed only weak fluorescence. H_2DCFDA signals began to accumulate in *mts3-1* 12h after the temperature upshift (Fig. S6). At that time point, the viability was high (~80%) so that fluorescence was not generated by dead cells. In VEG, there appeared to be no accumulation of ROS in *mts3-1* after the temperature upshift (viability =15%). The double staining *mts3-1* G0 cells with H_2DCFDA and Mitotracker showed that the strong signals of H2DCFDA were located in the mitochondria and nucleus (Fig. 3d), suggesting that ROS accumulated in the nucleus and mitochondria in *mts3-1* G0.

To explain results described above, we speculated that ROS was generated in G0 *mts3-1* due to the breakdown of mitochondria, but following results suggested that this was not the case. First, it was found that phenylmethylsulfonyl fluoride (PMSF), a serine protease inhibitor, when added to the culture, inhibited a decrease of Sdh2-GFP and Cox2 in G0 *mts3-1* (Fig. 4a). PMSF was reported to inhibit proteolysis in *S. pombe* vacuoles(31), so we examined the involvement of autophagy pathway. The double mutant of *mts3-1* and deletion Δ*atg8* was constructed (Atg8, LC3 homolog, is involved in autophagosome formation(32)) and observed using Sdh2-GFP as the marker of mitochondrial destruction. In the double mutant cells at 24h (37°C), the level of Sdh2-GFP did not decrease (Fig. 4b) and the mitochondrial degradation was virtually absent (Fig. 4c). These findings indicated that mitochondrial degradation in *mts3-1* required Atg8. A surprising outcome was the synthetic lethality of the double mutant in G0 as shown in Fig 4d. The viability of the double mutant sharply decreased after 12h and reached 3%, whereas more than 50% viability was maintained in the single *mts3-1*. Corroborating finding was that the accumulation of H_2DCFDA fluorescence was observed already in the double mutant at 6h whereas there was no accumulation in the single *mts3-1* at 6h (Fig. 4e). After 24h, fluorescence was much greater in the double mutant *mts3-1* Δ*atg8* than in *mts3-1*. As shown in Fig 4e and Fig. S7, H_2DCFDA signals were strong along the mitochondria in *mts3-1* Δ*atg8*, suggesting that autophagy actually caused the reduction of ROS (perhaps within mitochondria) by degrading mitochondria that was impaired in G0-phase *mts3-1*. In Δ*atg8* cells, the H_2DCFDA fluorescence was not significantly different from WT after 24h (Fig. S7). After longer incubation in G0 (two to three weeks) at 26°C, however, the fluorescence was stronger in Δ*atg8* cells, accompanied with the viability decrease after 21 days (Fig. S7). Therefore,

autophagy, though the degree is much less than proteasome function, is also required for long-term survival in G0. This is consistent with the previous report(31).

N-acetyl cysteine (NAC), an anti-oxidant, was added to the G0 culture to examine the effect on H_2DCFDA fluorescence (Fig. 4e). The fluorescence in *mts3-1*Δ*atg8* was significantly reduced after 6h and 24h. Consistently, the viability of the double mutant with NAC was much higher (83%, 47%, and 39%, respectively, at 20, 24, and 27 h) than the viability of double mutant without NAC (16%, 3%, and 0.3%, respectively, Fig. 4f). The severe lethality of the double mutant might thus be due to the abundance of ROS. Taken together, we concluded that mitochondrial degradation by autophagy is one of many anti-ROS protection events that occurred after proteasome dysfunction in G0 phase.

Discussion

A principal conclusion in this study is that *S. pombe* G0 cells require proteasome function during the maintenance of G0 quiescence. This conclusion was obtained using several ts mutants in the 26S proteasome subunits. Proteasome genes belong to the group of super housekeeping(6) because of their necessity for both proliferation and quiescence. Note that only 25% of the essential genes in VEG are also needed for G0 maintenance(6): many genes essential for proliferation such as cell division and DNA replication are not necessary for G0 maintenance. The second conclusion is that proteasome functions are quite different between G0 and VEG phase. This is based on striking defective phenotypes of proteasome mutants in G0 phase, regarding the huge increase of oxygen stress responsive compounds and the massive decrease of mitochondria that did not occur in VEG phase. How this difference is explained? The targets of proteasome may change from VEG to G0, more cytoplasmic ones in G0, which may lead to the export of proteasome to cytoplasm in G0 cells. In carbon starved cells of the fission yeast, the proteasome is also exported reversibly to the cytoplasm(33). Necessity of recycling proteins in G0(6) may require a number of cytoplasmic activities for proteasome, whilst in VEG events such as replication, rRNA transcription, mitosis and chromatin dynamics occur in the nucleus. Actual targets of proteasome in G0 remain to be clarified, however. In the quiescent/stationary phase of *Saccharomyces cerevisiae*, Aah1p (adenine deaminase) was reported as a substrate of the proteasome, while its proteolysis is not required for the maintenance of the quiescence(34).

The third, closely related to the second, conclusion of this study is that proteasome dysfunction in G0 elicits defensive responses, mainly the production of anti-oxidant components and the degradation of mitochondria by autophagy. These defensive responses were not found in VEG cells, suggesting that proteasome functions in G0 are directly or

indirectly involved in minimizing ROS. We provide evidence that viability loss in G0 is caused by the accumulation of oxidative stress. In addition, autophagy-mediated mitochondrial degradation as a matter of fact saved proteasome mutant G0 cells. In other word, proteasome collaborates with autophagy in supporting the longevity of G0 cells. Beside the loss of viability, physically aberrant structures were observed in G0 *mts3-1* mutant. Initially observed were the accumulation of electron-dense materials and the internal vesicles in the nucleus. At this timing, viability was high, suggesting that an abnormality in nuclear envelope or nuclear-cytoplasmic shuttling might be initial events that lead to the accumulation of ROS and mitochondrial dysfunction. Note that most of mitochondrial proteins are encoded by chromosomal genes. Aberrant mitochondria possibly producing a bulk of ROS then form, which in turn activate autophagy-dependent mitochondrial degradation. Our results are consistent with this hypothesis. Proteasome and autophagy seem to support life of non-dividing G0 phase cells (chronological life span). Our metabolomic and proteomic analyses identify anti-oxidant metabolites (glutathione, ergothioneine) and many ROS-defensive proteins that increase their levels in *mts3-1* G0 cells. In mammalian neurons, inactivation of the proteasome leads to ROS accumulation, mitochondrial injury and cell death (35-37), which are related to neurodegeneration. Injured mitochondria may be degraded by autophagy (mitophagy). Recent studies suggested that several proteins are involved in mitophagy, such as Atg32 (in budding yeast)(38, 39) and Park2 (E3 ligase responsible for Parkinson disease)(40, 41). Although neither of them has obvious homologues in *S.pombe*, there could be a common mechanism, by which injured mitochondria might be scavenged. Proteasome inhibitors, PS-519 and PS-341, are recently developed for the therapeutic purpose of inflammation and cancer such as multiple myeloma. The present results that proteasome dysfunction produces the autophagy-mediated degradation of mitochondria accompanying a number of defensive cellular functions against the elevated level of ROS, which may cause apoptotic removal of the drug-target mammalian cells, might explain some aspects of these drug effects.

Acknowledgements

We are greatly indebted to C. Gordon for *S. pombe* mutant strains, K. Gull, C. Gordon, and N. Bonnefoy for antibodies, K. Okamoto for discussion. K.T is supported by a JSPS, Grant-in-Aid for Scientific Research.

Figure legends

Fig. 1

Proteasome-enriched cytoplasm is required for the maintenance of G0 cells.
(a) Upper: proteasome localization in VEG and G0. α4 subunit and Histone H2A were tagged with green and red fluorescent protein, respectively. G0 cells (lower left, two round cells) and VEG cells (upper right, the rod-shaped cell) were independently prepared and mixed on a glass slide. Scale bar: 2.5μm. Lower: negative controls of no-GFP tagged strain. Scale bar: 5μm. **(b)** Time-course analysis of proteasome localization after –N. **(c)** Protein amounts in (b). α-TUB represents α-tubulin as a loading control. **(d)** Incubating G0 culture with 250 nM leptomycin B for 8 h induced a change in the proteasome localization from the cytoplasm to the nucleus. **(e)** The half-life of Cut8, a proteasome substrate, was examined in both G0 and VEG of WT and *mts3-1*. Proteins were extracted at the indicated time points after adding cycloheximide (100 μg/ml) and proteins were detected by immunoblotting. **(f)** The amount of poly-ubiquitinated proteins was examined in both WT and *mts3-1* mutants in G0. **(g)** The change of viabilities of WT and *mts3-1* were in G0. **(h-j)** TEM analysis of G0 cells (scale bars: 0.5μm). Arrow: an electron-dense deposit. Arrowhead: the lipid droplet in the nucleus. m: a mitochondrion (no mitochondria were visible in (i, j)). N: the nucleus. Insets show fluorescent images of chromosomal DNA stained by DAPI (scale bars: 2.5μm). **(k)** *mts3-1* mutant cells divided once after –N, whereas WT divided twice.

Fig. 2
The number of mitochondria was drastically decreased in proteasome mutants in G0.
(a) Mitochondria were visualized in G0 using Sdh2-GFP as a marker (green). Cell walls were stained by Calcofluor (white). Scale bar: 2 μm. **(b)** Mitochondrial protein amounts were decreased in *mts3-1* at restrictive temperature (37°C) in G0. 24* is the sample extracted from the culture at 26°C for 24h. **(c)** Mitochondria in VEG. **(d)** Sdh2-GFP levels remained constant at 37°C in VEG. **(e)** Scatter plot of emPAI values (protein abundance, see method) of proteins detected in two different extracts from WT cells, which were independently cultured at 37°C for 12h in G0. A part of the plot is enlarged in the inset to reveal each protein. Mitochondrial proteins are shown in green and others in blue. **(f)** Scatter plot of proteins abundance in both WT and *mts3-1* cells, which were cultured at 37°C for 12h in G0. For both strains, the experiments were repeated twice and the mean emPAI values were analyzed. The names of the proteins with the lowest levels in *mts3-1* are shown. **(g and h)** The same experiment as shown in (e and f) was performed in VEG.

Fig. 3
ROS accumulated in proteasome mutants in G0.

(a) The same experiment as shown in Fig. 2f. Purple, yellow and pale blue dots represent proteins, which are transcriptionally induced over 3-fold by H_2O_2, cadmium (Cd) and both of them, respectively. The proteins with the highest levels in *mts3-1* are indicated by numbers (1~4; see text). **(b)** Metabolic analysis revealed glutathione (reduced form; GSH) and ergothioneine in *mts3-1* in G0. Chromatogram patterns of each compound separated by HPLC. Values in red represent the integrated peak area (Y-axis). See text and materials. **(c)** The H_2DCFDA signal, an indicator of ROS, accumulated in *mts3-1* cells in G0, but not VEG. The time points shown are 0 h and 24h after the temperature shift to 37°C. The viability at each time point is also presented (%). Scale bar: 5μm. **(d)** The H_2DCFDA (green) signal accumulated in the nucleus (N) and mitochondria (m) in *mts3-1* cells 12h after the temperature shift. Mitochondria were stained by Mitotracker Orange (red). Scale bar: 2 μm.

Fig. 4

Autophagy is involved in degrading mitochondria to reduce the lethal accumulation of oxidative stress in G0.

(a) PMSF (2 mM) inhibited the decrease of mitochondrial proteins in *mts3-1* in G0. **(b)** Sdh2-GFP signals (green) maintained a tubular structure in the *mts3-1*Δ*atg8* double mutant, whereas the signal was greatly decreased in the *mts3-1* mutant. Both cells were cultured in G0 at 37°C for 24h. Scale bar: 2μm. **(c)** The amount of Sdh2-GFP proteins was kept constant in the *mts3-1*Δ*atg8* double mutant. **(d)** The viabilities of WT (blue), *mts3-1* (red), *mts3-1*Δ*atg8* (orange), and Δ*atg8* (green) were examined after the temperature shift to 37°C in G0. **(e)** The accumulation of oxidative stress was examined using H_2DCFDA. In the *mts3-1*Δ*atg8* double mutant, but not in *mts3-1*, stronger H_2DCFDA signals appeared 6 h after the temperature shift. At 24 h, the signal in the double mutant was still stronger than that in *mts3-1*. The addition of 30 mM N-acetyl cysteine (NAC) reduced H_2DCFDA signal intensity in the double mutant at 6 and 24 h. Scale bar: 4 μm. **(f)** NAC treatment rescued the viability of the *mts3-1*Δ*atg8* double mutant (orange solid triangle represents culture without NAC and orange empty triangle represents culture with NAC).

Methods

Strain, medium and culture

S. pombe heterothallic haploids 972h^- and 975h^+ and their derivatives were used. Complete YE and minimal EMM2 media were used to culture *S. pombe*(42). For G0 induction, exponentially growing cells at 26°C in EMM2 were harvested by vacuum filtration using a nitrocellulose membrane, washed with EMM2-N (EMM2 without nitrogen source), suspended in EMM2-N at a concentration of $2x10^6$ or $5x10^6$ cells/ml, and incubated for 24h at 26°C(4). To examine temperature-sensitive mutants, G0 cells of each strain were shifted from 26°C to 37°C.

Immunochemical methods

For immunoblot analysis, total proteins were extracted using the trichloroacetic acid (TCA) method. Identical amounts of proteins were separated by SDS-PAGE gel and blotted to nitrocellulose membranes. Anti-Cut8, anti-Pad1, anti-Hxk2, anti-Cox2 (a gift from Dr. Bonnefoy), anti-α-tubulin (TAT1; a gift from Dr. Gull), anti-GFP (Roche), and anti-FLAG (Sigma) antibodies were used as primary antibodies. Horseradish peroxidase-conjugated secondary antibodies and an ECL chemiluminescence system (Amersham) were used to amplify signal expression.

Proteomics and metabolite analysis

To identify immunoprecipitated proteins, we used the procedure reported by Hayashi et al, with some modifications(22). For whole proteome analysis, total proteins were extracted, separated by SDS-PAGE, in-gel-digested and analyzed with LC-MS/MS. All MS/MS spectra were searched against an *S. pombe* non-redundant protein database with the Mascot program (Matrix Science, London, UK). The output data from Mascot was analyzed using in-house software to select reliable peptides and calculate emPAI values(23). For metabolite analysis, we followed methods described previously(28). See Methods. S1 for the detailed methods.

Microscopy

All images were acquired using an AxioPlan 2 (Zeiss) or DeltaVision microscope setup. For mitochondrial staining, Mitotracker GreenFM and Mitotracker Orange (Invitrogen) were used(20). To obtain mitochondrial images in whole cells, we scanned 21 Z-axis sections at a 0.2-μm interval and the obtained images were deconvolved and projected on a 2D plane. For oxidative stress staining via H_2DCFDA (Invitrogen), we followed the method reported(30). For TEM analysis, see Methods. S1 for the detailed methods.

References

1. **Zetterberg A & Larsson O (1985) Kinetic analysis of regulatory events in G1 leading to proliferation or quiescence of Swiss 3T3 cells. *Proc Natl Acad Sci U S A* 82(16):5365-5369.**
2. **Wullschleger S, Loewith R, & Hall MN (2006) TOR signaling in growth and metabolism. *Cell* 124(3):471-484.**
3. **Gray JV, *et al.* (2004) "Sleeping beauty": quiescence in Saccharomyces cerevisiae. *Microbiol Mol Biol Rev* 68(2):187-206.**
4. **Su SS, Tanaka Y, Samejima I, Tanaka K, & Yanagida M (1996) A nitrogen starvation-induced dormant G0 state in fission yeast: the establishment from uncommitted G1 state and its delay for return to proliferation. *J Cell Sci* 109 (Pt 6):1347-1357.**
5. **Shimanuki M, *et al.* (2007) Two-step, extensive alterations in the transcriptome from G0 arrest to cell division in Schizosaccharomyces pombe. *Genes Cells* 12(5):677-692.**
6. **Sajiki K, *et al.* (2009) Genetic control of cellular quiescence in S. pombe. *J Cell Sci* 122(Pt 9):1418-1429.**
7. **Hershko A & Ciechanover A (1998) The ubiquitin system. *Annu Rev Biochem* 67:425-479.**
8. **Gordon C, McGurk G, Wallace M, & Hastie ND (1996) A conditional lethal mutant in the fission yeast 26 S protease subunit mts3+ is defective in metaphase to anaphase transition. *J Biol Chem* 271(10):5704-5711.**
9. **Sudakin V, *et al.* (1995) The cyclosome, a large complex containing cyclin-selective ubiquitin ligase activity, targets cyclins for destruction at the end of mitosis. *Mol Biol Cell* 6(2):185-197.**
10. **Yamashita YM, *et al.* (1996) 20S cyclosome complex formation and proteolytic activity inhibited by the cAMP/PKA pathway. *Nature* 384(6606):276-279.**
11. **Funabiki H, *et al.* (1997) Fission yeast Cut2 required for anaphase has two destruction boxes. *EMBO J* 16(19):5977-5987.**
12. **Yamano H, Gannon J, & Hunt T (1996) The role of proteolysis in cell cycle progression in Schizosaccharomyces pombe. *EMBO J* 15(19):5268-5279.**
13. **Zachariae W, Shin TH, Galova M, Obermaier B, & Nasmyth K (1996) Identification of subunits of the anaphase-promoting complex of Saccharomyces cerevisiae. *Science* 274(5290):1201-1204.**
14. **Wilkinson CR, *et al.* (1998) Localization of the 26S proteasome during mitosis**

and meiosis in fission yeast. *Embo J* 17(22):6465-6476.

15. **Tatebe H & Yanagida M (2000) Cut8, essential for anaphase, controls localization of 26S proteasome, facilitating destruction of cyclin and Cut2. *Curr Biol* 10(21):1329-1338.**
16. **Takeda K & Yanagida M (2005) Regulation of nuclear proteasome by Rhp6/Ubc2 through ubiquitination and destruction of the sensor and anchor Cut8. *Cell* 122(3):393-405.**
17. **Fukuda M, *et al.* (1997) CRM1 is responsible for intracellular transport mediated by the nuclear export signal. *Nature* 390(6657):308-311.**
18. **Leggett DS, *et al.* (2002) Multiple associated proteins regulate proteasome structure and function. *Mol Cell* 10(3):495-507.**
19. **Zhang Q, *et al.* (2003) Schizosaccharomyces pombe cells deficient in triacylglycerols synthesis undergo apoptosis upon entry into the stationary phase. *J Biol Chem* 278(47):47145-47155.**
20. **Pozniakovsky AI, *et al.* (2005) Role of mitochondria in the pheromone- and amiodarone-induced programmed death of yeast. *J Cell Biol* 168(2):257-269.**
21. **Ramos PC, Hockendorff J, Johnson ES, Varshavsky A, & Dohmen RJ (1998) Ump1p is required for proper maturation of the 20S proteasome and becomes its substrate upon completion of the assembly. *Cell* 92(4):489-499.**
22. **Hayashi T, *et al.* (2007) Rapamycin sensitivity of the Schizosaccharomyces pombe tor2 mutant and organization of two highly phosphorylated TOR complexes by specific and common subunits. *Genes Cells* 12(12):1357-1370.**
23. **Ishihama Y, *et al.* (2005) Exponentially modified protein abundance index (emPAI) for estimation of absolute protein amount in proteomics by the number of sequenced peptides per protein. *Mol Cell Proteomics* 4(9):1265-1272.**
24. **Taricani L, Feilotter HE, Weaver C, & Young PG (2001) Expression of hsp16 in response to nucleotide depletion is regulated via the spc1 MAPK pathway in Schizosaccharomyces pombe. *Nucleic Acids Res* 29(14):3030-3040.**
25. **Chen D, *et al.* (2003) Global transcriptional responses of fission yeast to environmental stress. *Mol Biol Cell* 14(1):214-229.**
26. **Brendel C, Gelman L, & Auwerx J (2002) Multiprotein bridging factor-1 (MBF-1) is a cofactor for nuclear receptors that regulate lipid metabolism. *Mol Endocrinol* 16(6):1367-1377.**
27. **Monroe RK & Halvorsen SW (2009) Environmental toxicants inhibit neuronal Jak tyrosine kinase by mitochondrial disruption. *Neurotoxicology* 30(4):589-598.**

28. Pluskal T, Nakamura, T., Villar-Briones, A. and Yanagida, M. (2010) Metabolic profiling of the fission yeast S. pombe: quantification of compounds under different temperatures and genetic perturbation. *Mol. BioSyst.* DOI:10.1039/b908784b

29. Chaudiere J & Ferrari-Iliou R (1999) Intracellular antioxidants: from chemical to biochemical mechanisms. *Food Chem Toxicol* 37(9-10):949-962.

30. Marchetti MA, Weinberger M, Murakami Y, Burhans WC, & Huberman JA (2006) Production of reactive oxygen species in response to replication stress and inappropriate mitosis in fission yeast. *J Cell Sci* 119(Pt 1):124-131.

31. Kohda TA, *et al.* (2007) Fission yeast autophagy induced by nitrogen starvation generates a nitrogen source that drives adaptation processes. *Genes Cells* 12(2):155-170.

32. Kirisako T, *et al.* (1999) Formation process of autophagosome is traced with Apg8/Aut7p in yeast. *J Cell Biol* 147(2):435-446.

33. Laporte D, Salin B, Daignan-Fornier B, & Sagot I (2008) Reversible cytoplasmic localization of the proteasome in quiescent yeast cells. *J Cell Biol* 181(5):737-745.

34. Escusa S, Camblong J, Galan JM, Pinson B, & Daignan-Fornier B (2006) Proteasome- and SCF-dependent degradation of yeast adenine deaminase upon transition from proliferation to quiescence requires a new F-box protein named Saf1p. *Mol Microbiol* 60(4):1014-1025.

35. Qiu JH, *et al.* (2000) Proteasome inhibitors induce cytochrome c-caspase-3-like protease-mediated apoptosis in cultured cortical neurons. *J Neurosci* 20(1):259-265.

36. Ling YH, Liebes L, Zou Y, & Perez-Soler R (2003) Reactive oxygen species generation and mitochondrial dysfunction in the apoptotic response to Bortezomib, a novel proteasome inhibitor, in human H460 non-small cell lung cancer cells. *J Biol Chem* 278(36):33714-33723.

37. Papa L & Rockwell P (2008) Persistent mitochondrial dysfunction and oxidative stress hinder neuronal cell recovery from reversible proteasome inhibition. *Apoptosis* 13(4):588-599.

38. Okamoto K, Kondo-Okamoto N, & Ohsumi Y (2009) Mitochondria-anchored receptor Atg32 mediates degradation of mitochondria via selective autophagy. *Dev Cell* 17(1):87-97.

39. Kanki T, Wang K, Cao Y, Baba M, & Klionsky DJ (2009) Atg32 is a mitochondrial protein that confers selectivity during mitophagy. *Dev Cell*

17(1):98-109.

40. Shimura H*, et al.* (2000) Familial Parkinson disease gene product, parkin, is a ubiquitin-protein ligase. *Nat Genet* 25(3):302-305.

41. Narendra D, Tanaka A, Suen DF, & Youle RJ (2008) Parkin is recruited selectively to impaired mitochondria and promotes their autophagy. *J Cell Biol* 183(5):795-803.

42. Moreno S, Klar A, & Nurse P (1991) Molecular genetic analysis of fission yeast Schizosaccharomyces pombe. *Methods Enzymol* 194:795-823.

Fig. 1

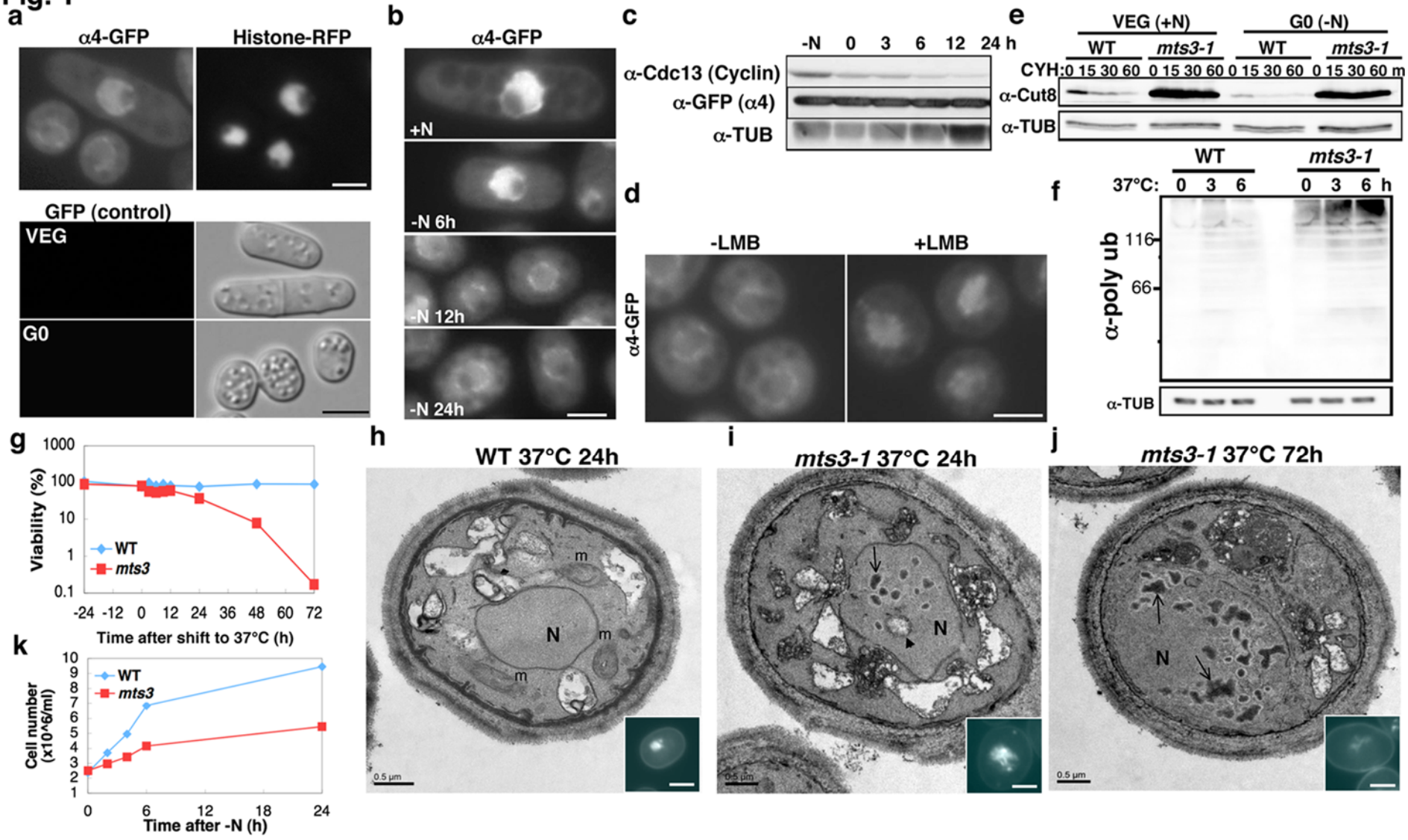
a
α4-GFP
Histone-RFP
GFP (control)
VEG
G0
b
α4-GFP
+N
-N 6h
-N 12h
-N 24h
c
-N 0 3 6 12 24 h
α-Cdc13 (Cyclin)
α-GFP (α4)
α-TUB
d
-LMB
+LMB
α4-GFP
e
VEG (+N)
G0 (-N)
WT
mts3-1
WT
mts3-1
CYH: 0 15 30 60 0 15 30 60 0 15 30 60 0 15 30 60 m
α-Cut8
α-TUB
f
WT
mts3-1
37°C: 0 3 6 0 3 6 h
α-poly ub
116
66
α-TUB
g
Viability (%)
1000
100
10
1
0.1
WT
mts3
-24 -12 0 12 24 36 48 60 72
Time after shift to 37°C (h)
k
Cell number (x10^6/ml)
10
9
8
7
6
5
4
3
2
1
WT
mts3
0 6 12 18 24
Time after -N (h)
h
WT 37°C 24h
m
N
m
m
0.5 μm
i
mts3-1 37°C 24h
N
0.5 μm
j
mts3-1 37°C 72h
N
0.5 μm

Fig. 2

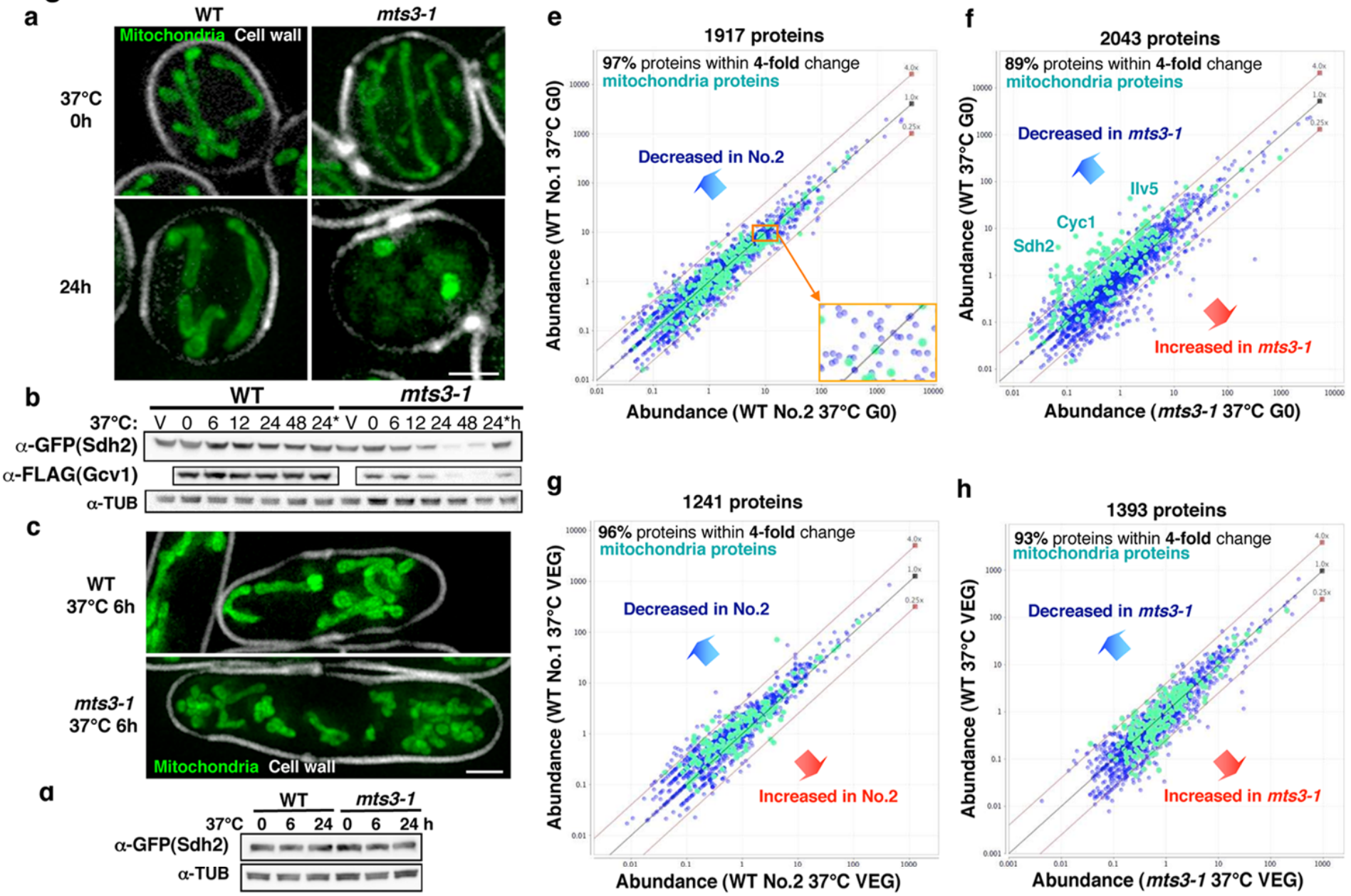
a
WT
mts3-1
Mitochondria
Cell wall
37°C
0h
24h
b
WT
mts3-1
37°C: V 0 6 12 24 48 24* V 0 6 12 24 48 24*h
α-GFP(Sdh2)
α-FLAG(Gcv1)
α-TUB
c
WT
37°C 6h
mts3-1
37°C 6h
Mitochondria
Cell wall
d
WT
mts3-1
37°C 0 6 24 0 6 24 h
α-GFP(Sdh2)
α-TUB
e
1917 proteins
97% proteins within 4-fold change
mitochondria proteins
Decreased in No.2
Abundance (WT No.1 37°C G0)
Abundance (WT No.2 37°C G0)
f
2043 proteins
89% proteins within 4-fold change
mitochondria proteins
Decreased in mts3-1
Ilv5
Cyc1
Sdh2
Increased in mts3-1
Abundance (WT 37°C G0)
Abundance (mts3-1 37°C G0)
g
1241 proteins
96% proteins within 4-fold change
mitochondria proteins
Decreased in No.2
Increased in No.2
Abundance (WT No.1 37°C VEG)
Abundance (WT No.2 37°C VEG)
h
1393 proteins
93% proteins within 4-fold change
mitochondria proteins
Decreased in mts3-1
Increased in mts3-1
Abundance (WT 37°C VEG)
Abundance (mts3-1 37°C VEG)

Fig. 3

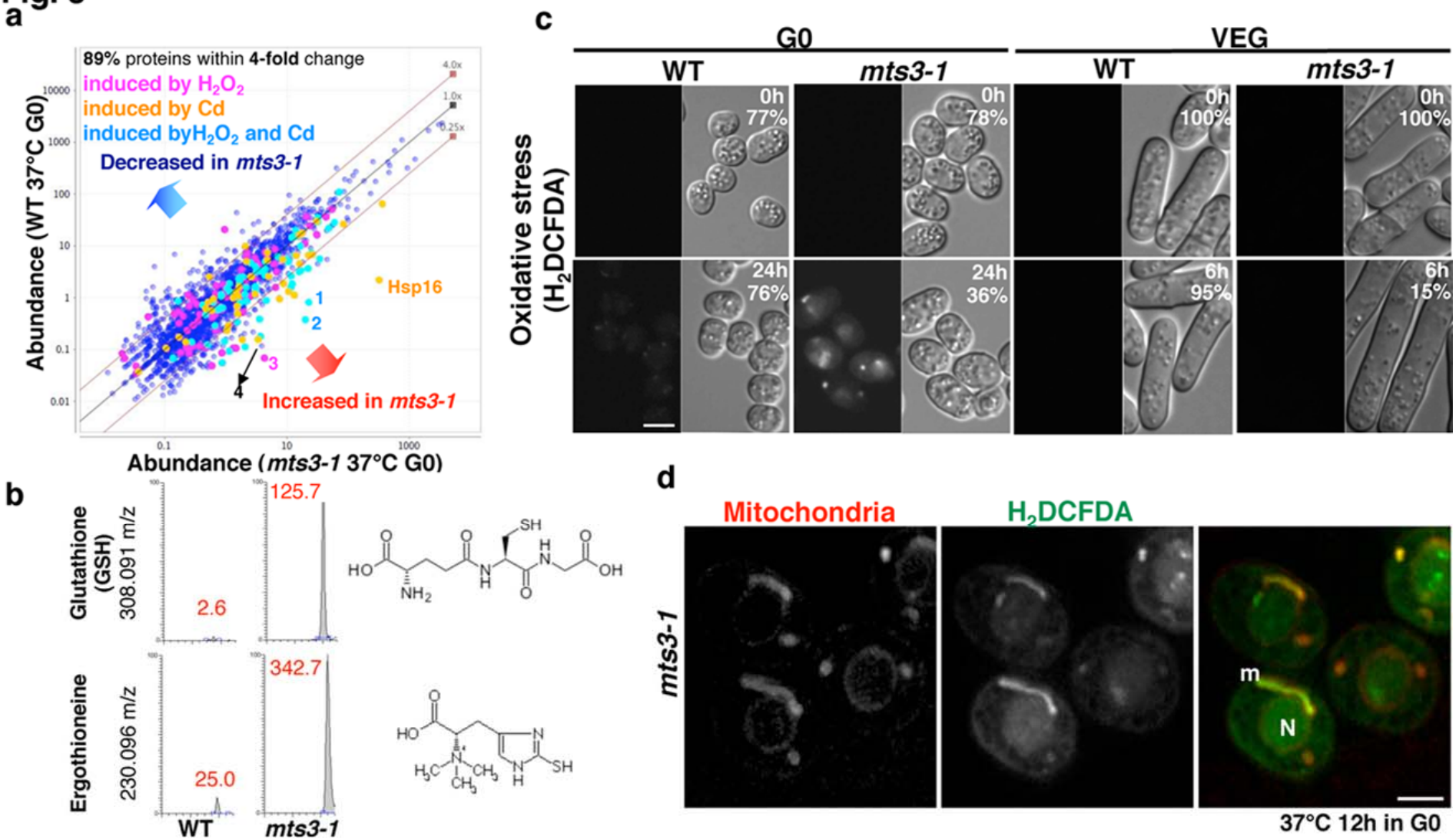
a
89% proteins within 4-fold change
induced by H_2O_2
induced by Cd
induced byH_2O_2 and Cd
Decreased in mts3-1
Increased in mts3-1
Hsp16
1
2
3
4
Abundance (WT 37°C G0)
Abundance (mts3-1 37°C G0)
b
Glutathione (GSH) 308.091 m/z
125.7
2.6
Ergothioneine 230.096 m/z
342.7
25.0
WT
mts3-1
c
G0
VEG
WT
mts3-1
WT
mts3-1
Oxidative stress (H_2DCFDA)
0h 77%
0h 78%
0h 100%
0h 100%
24h 76%
24h 36%
6h 95%
6h 15%
d
Mitochondria
H_2DCFDA
mts3-1
m
N
37°C 12h in G0

Fig. 4

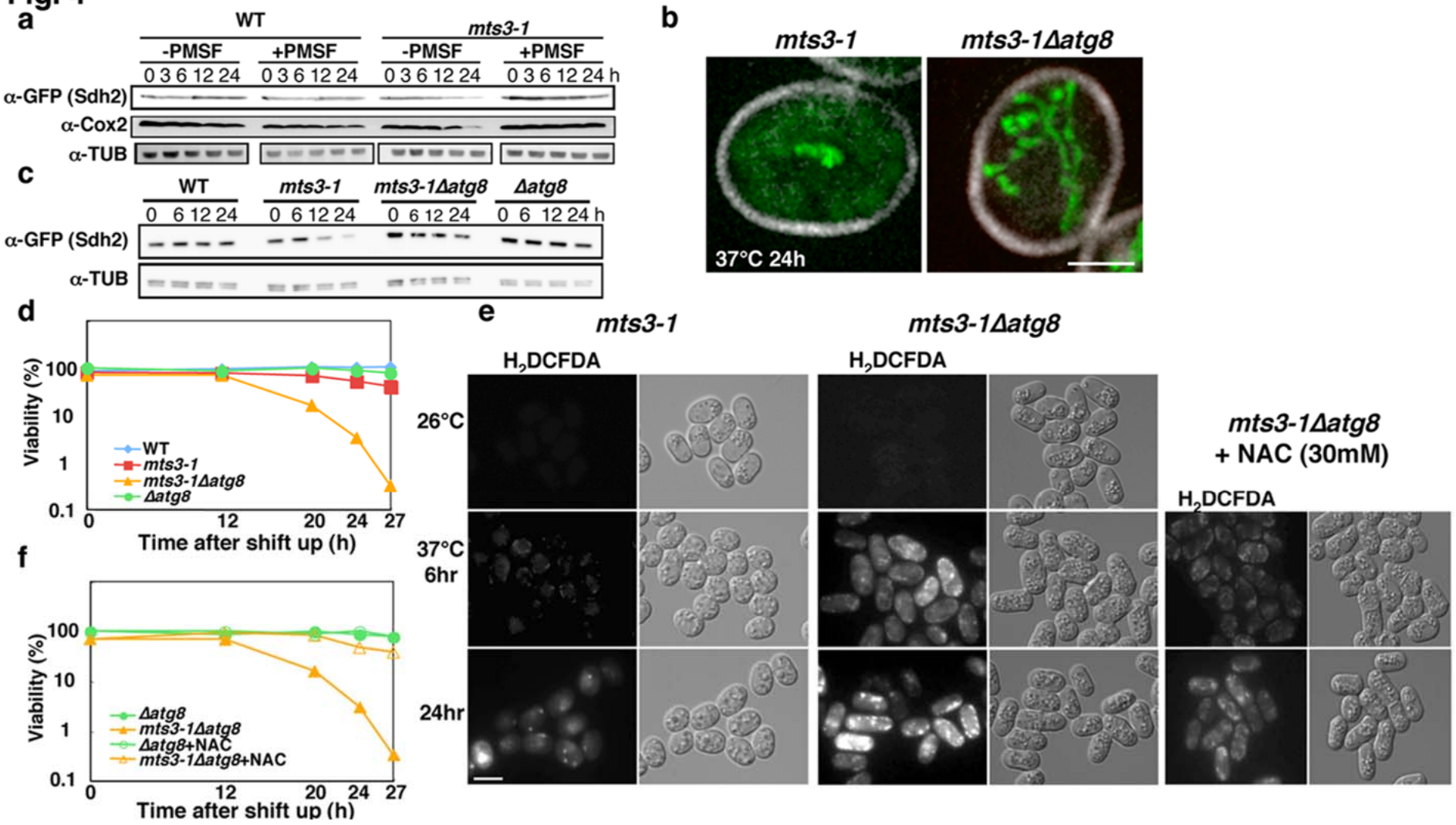
a
WT
mts3-1
-PMSF
+PMSF
-PMSF
+PMSF
0 3 6 12 24 0 3 6 12 24 0 3 6 12 24 0 3 6 12 24 h
α-GFP (Sdh2)
α-Cox2
α-TUB
b
mts3-1
mts3-1Δatg8
37°C 24h
c
WT
mts3-1
mts3-1Δatg8
Δatg8
0 6 12 24 0 6 12 24 0 6 12 24 0 6 12 24 h
α-GFP (Sdh2)
α-TUB
d
Viability (%)
100
10
1
0.1
WT
mts3-1
mts3-1Δatg8
Δatg8
0 12 20 24 27
Time after shift up (h)
e
mts3-1
mts3-1Δatg8
H2DCFDA
H2DCFDA
mts3-1Δatg8
+ NAC (30mM)
H2DCFDA
26°C
37°C
6hr
24hr
f
Viability (%)
100
10
1
0.1
Δatg8
mts3-1Δatg8
Δatg8+NAC
mts3-1Δatg8+NAC
0 12 20 24 27
Time after shift up (h)

Figure legends for Supporting Information

Fig. S1

(a) The localization of Pad1 (Rpn11)-GFP changed during the transition from VEG to G0. As shown in Fig. 1a, Pad1-GFP was localized to the nucleus and the nuclear periphery, although the nuclear signal was diminished and the signal in the cytoplasm was increased. The signal in the nuclear periphery remained detectable in G0. Scale bar: 2 μm. (b) *mts3-1* mutant cells kept the viability high until ten days after –N at 26°C. (c) The temperature sensitive mutant of Pad1/Rpn11 subunit of 19S complex, *pad1-932*, lost the viability at the restrictive temperature (37°C) in G0.

Fig. S2

(a) The α4-FLAGx3 protein expressed by the chromosomally integrated gene under the native promoter was immunoprecipitated and analyzed by sodium dodecyl sulfate-polyacrylamide gel electrophoresis. The 20 gel slices of G0 and VEG lanes were analyzed by LC/MS/MS after tryptic digestion. The names of the detected subunits or accessory proteins of the proteasome are shown. Blue represents 19S subunits and red represents 20S complex subunits. Black indicates accessory proteins. The experiments were repeated three times and the typical result is shown. (b) List of detected subunits and accessory proteins. Two Rpn13 homologues were observed in *S. pombe*.

Fig. S3

Nile red stained a structure in the nucleus, which could be the vesicle-like structure observed in TEM analysis. *mts3-1* cells were stained by Nile red and Hochst33342 12h after the temperature shift to 37°C in G0. The signals indicated by the arrow were localized in the nucleus, which was stained by Hochst33342. Twenty-one images at 0.2-μm intervals on the Z-axis were acquired using the DeltaVision system. One central section is shown after digital image processing. Scale bar: 2 μm.

Fig. S4

(a) Mitotracker GreenFM staining showed a decreased number of mitochondria in *mts3-1* at the restrictive temperature (37°C) in G0. Scale bar: 2 μm. (b) Mitochondria were visualized by Sdh2-GFP tagging. In *mts3-1* cells, mitochondria were largely decreased at the restrictive temperature (37°C 24h) in G0. (c) In this study, we

isolated four temperature sensitive mutants of proteasome from Hayashi mutant library in our laboratory. All mutants showed a decrease in the number of mitochondria in G0. Sdh2-GFP was used as a mitochondrial marker. In mutants, Sdh2-GFP signals were significantly reduced 24 h after the temperature shift. Weaker signals in the cytoplasm might be GFP signals indicating incorporation of the GFP into vacuoles by autophagy. Scale bar: 2 μm. (d) Western blotting showed that Cox2 protein decreased in proteasome mutants.

Fig. S5

Glutathione and ergothioneine detected by LC/MS were increased not only in *mts3-1*, but also in *pts1-727*, the newly-identified 20S proteasome mutant (see Supplementary figure 5). Trimethyl-histidine, a precursor of ergothioneine, was also increased in *mts3* and *pts1*.

Fig. S6

H2DCFDA fluorescence began to accumulate in *mts3-1* 12h (red line) after the temperature shift to 37°C in G0. Scale bar: 5 μm.

Fig. S7

(a) In the *mts3-1* Δ*atg8* double mutant, H_2DCFDA fluorescent signal was strong in the mitochondria. The double mutant cells were simultaneously stained with H_2DCFDA and Mitotracker Orange (12h after shift to 37°C in G0). Scale bar: 4 μm. (b) In Δ*atg8* cells, no significant accumulation of ROS was observed 24h after temperature-shift up in G0. Figures of *mts3-1* and *mts3-1* Δ*atg8* are same as Fig. 4. Scale bar: 4 μm. (c) ROS was accumulated in Δ*atg8* cells fourteen days after G0 entry at 26°C. Scale bar: 5μm. (d) Δ*atg8* cells lost the viability after 21 days in G0. The averages of viabilities of three independent experiments were shown. (Error bars: S.D.)

Table. S1

The list of proteins for which the emPAI ratio (*mts3*/WT) decreased to less than 0.25-fold in *mts3-1* in G0. Mitochondrial residents are shown in green. Sixty of 125 decreased proteins were mitochondrial.

Table. S2

The list of proteins for which the emPAI ratio (*mts3*/WT) increased over 4.0-fold in *mts3-1* in G0. Genes, which are transcriptionally induced over 3-fold by H_2O_2, Cadmium (Cd) and both of them, are represented by purple, yellow and blue, respectively. SPBC83.17 (Mbf1 indicated by the asterisk)) is induced by heat (>5.0-fold) and Cd (~2.5-fold).

Supplementary Method. S1

Proteomics

To identify immunoprecipitated proteins, we used the procedure reported by Hayashi et al, with some modifications(22). For whole proteome analysis, total *S. pombe* proteins were extracted from G0 or VEG cells by TCA precipitation. TCA solution (100%) was added to cell cultures at a final concentration of 20% and cells were harvested by centrifugation at 4°C. Harvested cells were crushed in 10% TCA solution using glass beads and Multi-beads shocker (Yasui Kikai, Osaka, Japan) and proteins were precipitated by centrifugation at 14,000 x 15min. Precipitants were boiled in 1x LDS buffer (Invitrogen) with 0.16 M Tris and β-mercaptoethanol at 70°C for 10 min. Boiled samples were centrifuged at 14,000 rpm for 5 min to remove cell debris and were quantified using a Bradford assay kit (Bio Rad). An aliquot (33μg) of each sample was separated by NuPAGE Bis-Tris gel (4-12%), stained with Coomassie brilliant blue and sliced into 20 strips from the well to the dye front. After in-gel digestion with modified trypsin (Roche, Nutley, NJ), the resulting peptides were analyzed with online LC-MS/MS on a Finnegan LTQ (Thermo Fischer). All MS/MS spectra were searched against an *S. pombe* non-redundant protein database (including common contaminants such as trypsin and keratin) with the Mascot program (Matrix Science, London, UK). The output data from Mascot was analyzed using in-house software to select reliable peptides and calculate emPAI values(23). The emPAI values are calculated from 10^{PAI}-1 (PAI = observed peptide number / observable peptide number). The obtained data were applied to in-house software to draw scatter plots.

Metabolite analysis

We followed methods described previously(28). Liquid cell culture (50 ml/sample) was filtered using an Omnipore membrane filter (Millipore) and collected cells were

immediately placed into -40ºC MeOH. Cell membranes were disrupted using glass beads and a multi-bead shocker in 50% MeOH at 0ºC. Proteins were removed from the extracts by filtering on an Amicon Ultra 10-kDa cut-off filter (Millipore) for 60 min at 4ºC. Sample solvent was evaporated by centrifugation on a vacuum concentrator (TOMY CC-105) for 60 min and the remaining liquid was re-suspended into 40 µl 50% acetonitrile by gentle pipetting. Samples were then analyzed by LC-MS using a Paradigm MS4 HPLC system (Michrom Bioresources) coupled to an LTQ Orbitrap mass spectrometer (Thermo Fisher Scientific). LC separation was performed on a ZIC-pHILIC column (Merck SeQuant; 150 x 2.1 mm, 5 µm particle size) using gradient elution with acetonitrile (A) and 10 mM ammonium carbonate + 0.2% ammonium hydroxide (B) as the mobile phase. For MS detection, an electrospray ionization source was used and operated in positive ionization mode with 4 kV spray voltage. Pure ergothioneine and GSH standards were obtained and analyzed for verification of metabolite m/z and retention time.

Electron microscopy

For TEM analysis, cells were fixed with 2% glutaraldehyde in 100 mM phosphate buffer pH 7.2 for 2 h at 26ºC, post-fixed with 2% potassium permanganate overnight at 4ºC, and embedded in Epon812 (TAAB). Ultra-thin sections were stained in 2% uranyl acetate and Reynold's lead citrate, and viewed with a TEM JEM1230R (JEOL) operating at 100kV.

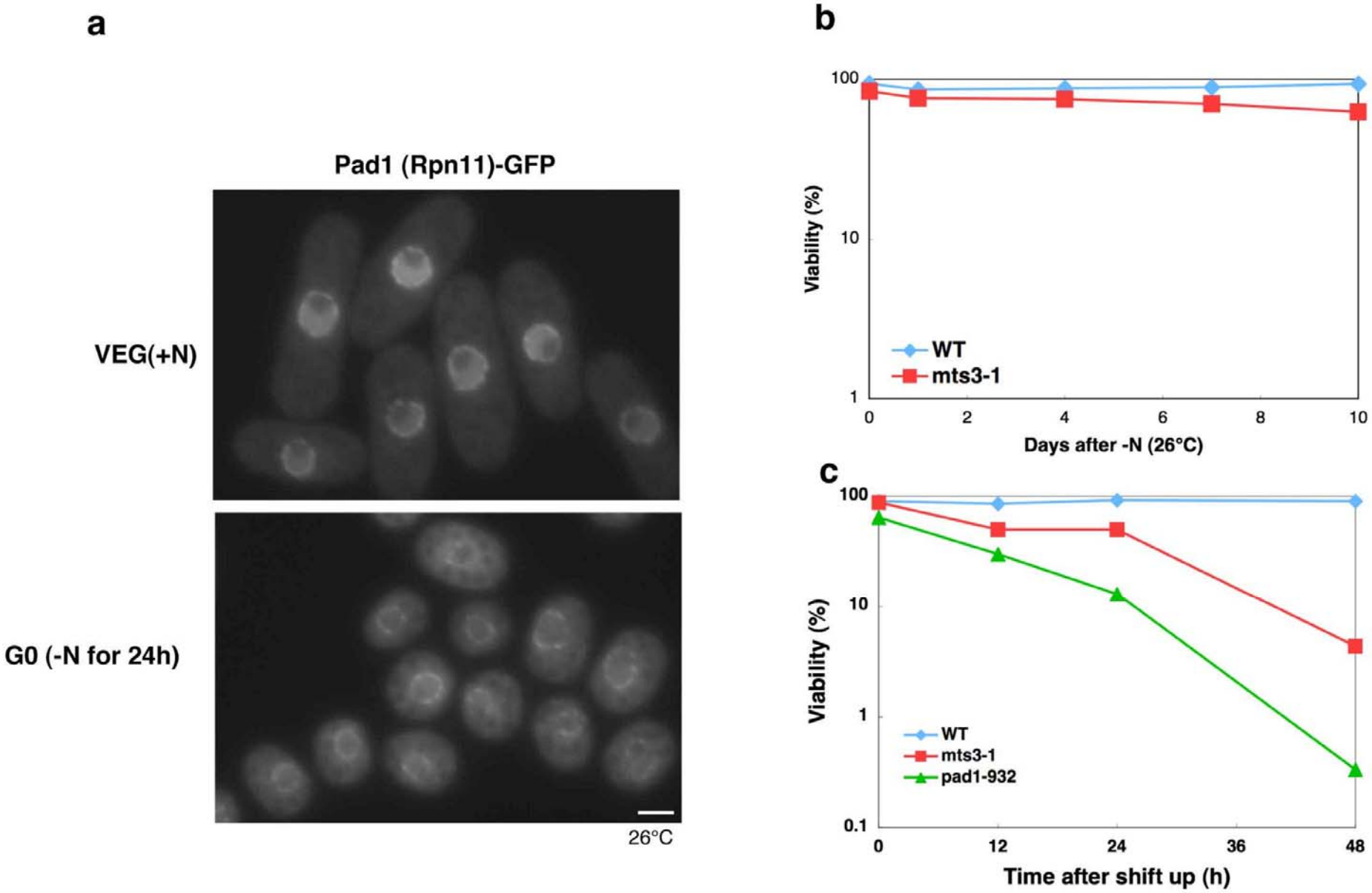
a
Pad1 (Rpn11)-GFP
VEG(+N)
G0 (-N for 24h)
26°C
b
100
10
1
Viability (%)
WT
mts3-1
0
2
4
6
8
10
Days after -N (26°C)
c
100
10
1
0.1
Viability (%)
WT
mts3-1
pad1-932
0
12
24
36
48
Time after shift up (h)

a

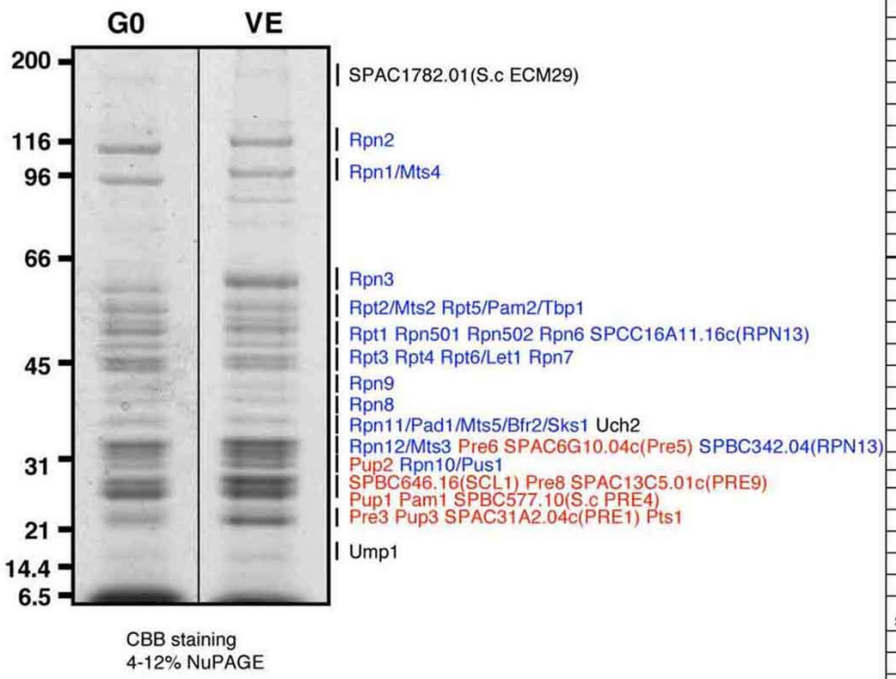

CBB staining
4-12% NuPAGE

b

Systematic name / name	*S.cerevisiae* homologue	Identified peptides		Coverage (%)		MW (kDa)	Function
		G0	Veg	G0	Veg		
SPBC646.16	SCL1	41	26	94	71	27	20S alpha 1
SPCC1442.06/pre8	PRE8	26	17	98	60	26	20S alpha 2
SPAC13C5.01c	PRE9	30	22	88	65	28	20S alpha 3
SPBC106.16/pre6	PRE6	29	32	68	68	28	20S alpha 4
SPAC323.02c/pup2	PUP2	33	28	79	71	28	20S alpha 5
SPAC6G10.04c	PRE5	46	42	75	74	30	20S alpha 6
SPCC1795.04c/pre10	PRE10	21	19	48	43	28	20S alpha 7
SPBC4C3.10c /pre3	PRE3	31	29	81	90	25	20S beta 1
SPAC23D3.07/pup1	PUP1	29	18	58	42	29	20S beta 2
SPCC63.12c/pup3	PUP3	8	9	25	34	23	20S beta 3
SPAC31A2.04c	PRE1	10	11	49	61	22	20S beta 4
SPAC4A8.13c/pts1	PRE2	21	19	61	61	30	20S beta 5
SPAC22F8.06/pam1	PRE7	28	20	72	61	25	20S beta 6
SPBC577.10	PRE4	27	16	78	59	29	20S beta 7
SPBC16C6.07c	RPT1	43	35	77	68	49	19S Base
SPBC4.07c/mts2/rpt2	RPT2	45	28	68	54	50	19S Base
SPCC576.10c/rpt3	RPT3	26	24	51	51	44	19S Base
SPCC1682.16/rpt4	RPT4	37	34	69	66	44	19S Base
SPAC3A11.12c/rpt5/pam2/tbp1	RPT5	38	32	54	52	49	19S Base
SPBC23G7.12c/rpt6/let1	RPT6	34	33	69	65	45	19S Base
SPBP19A11.03c/rpn1/mts4	RPN1	65	51	56	52	98	19S Base
SPBC17D11.07/rpn2	RPN2	88	63	59	49	107	19S Base
SPBC119.01/rpn3	RPN3	38	27	53	44	57	19S lid
SPAC1420.03/rpn501/rpn5-a*							
SPAPB8E5.02c/rpn502/rpn5-b*	RPN5	39	28	59	54	52	19S lid
SPAC23G3.11/Rpn6	RPN6	28	21	55	44	47	19S lid
SPBC582.07c/rpn7	RPN7	34	28	57	52	47	19S lid
SPCC1682.10/rpn8	RPN8	21	11	67	34	36	19S lid
SPAC607.05/rpn9	RPN9	35	20	71	41	43	19S lid
SPAC637.10c/rpn10/pus1	RPN10	13	8	43	38	27	19S lid
SPAC31G5.13/rpn11/pad1/sks1/bfr2/mts5	RPN11	25	17	56	55	35	19S lid
SPBC16G5.01/rpn12/mts3	RPN12	24	14	64	41	31	19S lid
SPCC16A11.16c#	RPN13	10	10	19	20	44	19S lid
SPBC342.04#	RPN13	5	5	9.3	22	32	19S lid
SPCC14G10.03c/ump1	UMP1	13	10	49	48	15	20S assembly
SPBC409.06/uch2	YUH1	21	14	52	39	34	Ub C-terminal hydlase
SPAC1782.01	ECM29	23	18	14	12	191	stabilizing 26S

*: There are two homologues of Rpn5.
#: There are two homologues of Rpn13.

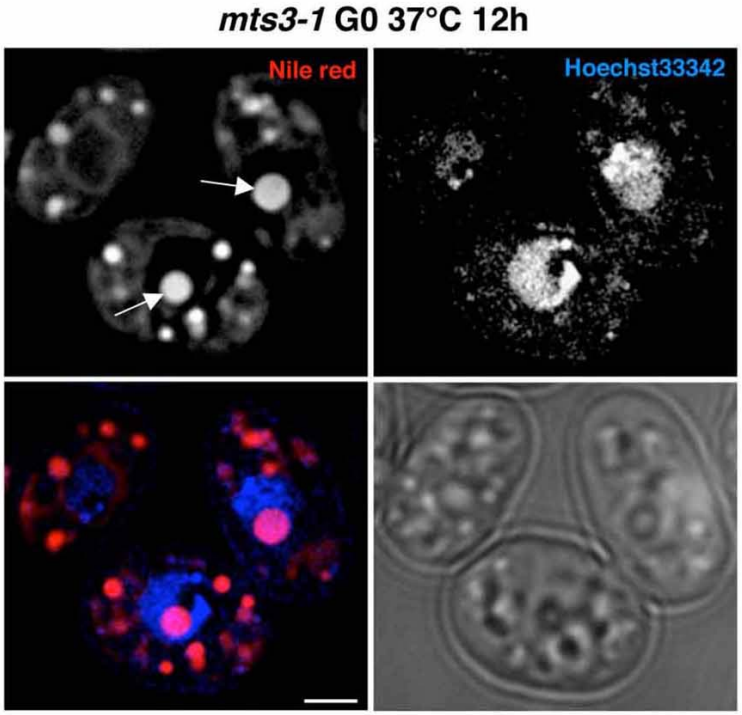
mts3-1 G0 37°C 12h
Nile red
Hoechst33342

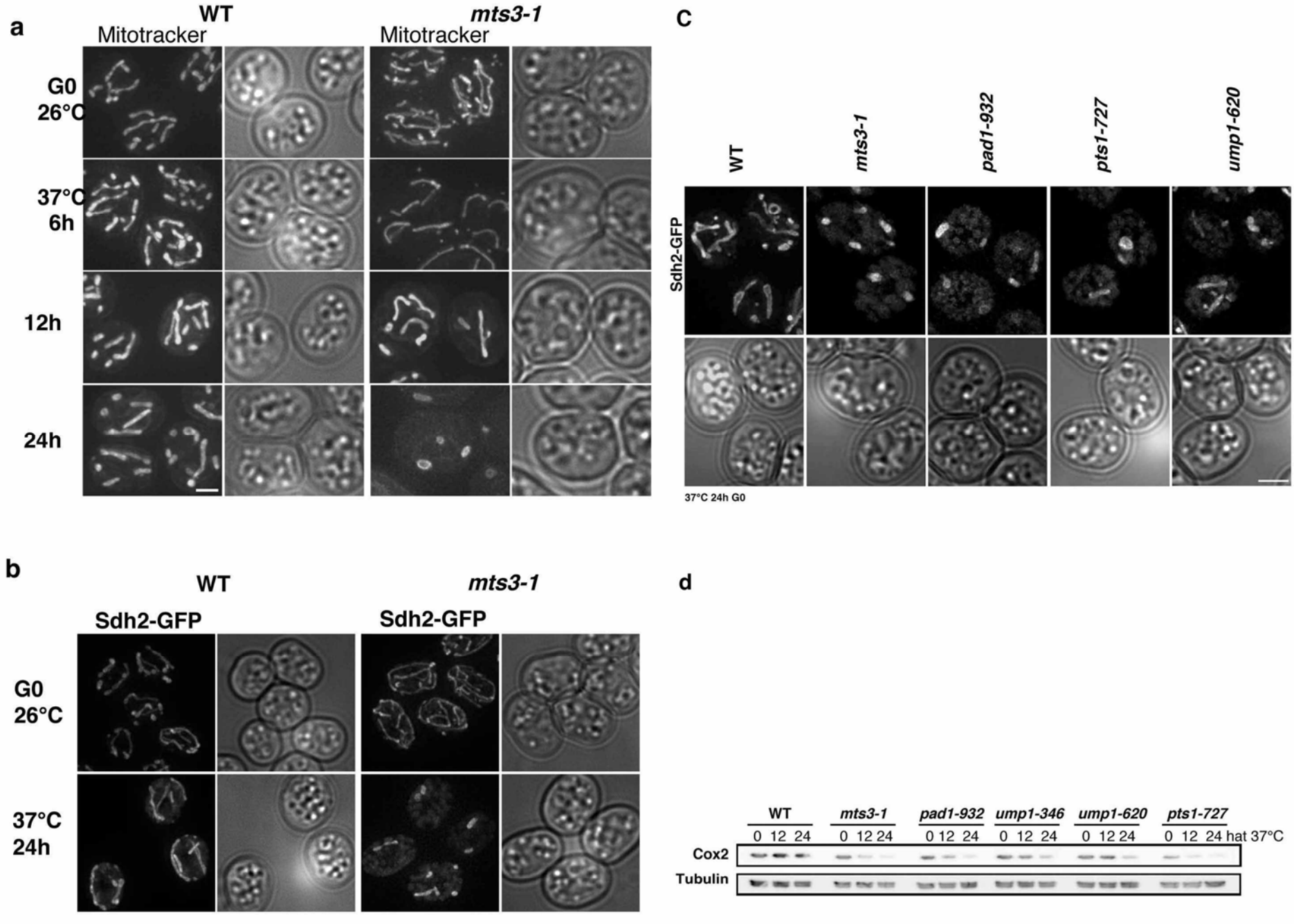
a
WT
mts3-1
Mitotracker
Mitotracker
G0
26°C
37°C
6h
12h
24h
b
WT
mts3-1
Sdh2-GFP
Sdh2-GFP
G0
26°C
37°C
24h
c
WT
mts3-1
pad1-932
pts1-727
ump1-620
Sdh2-GFP
37°C 24h G0
d
WT
mts3-1
pad1-932
ump1-346
ump1-620
pts1-727
0 12 24
0 12 24
0 12 24
0 12 24
0 12 24
0 12 24 hat 37°C
Cox2
Tubulin

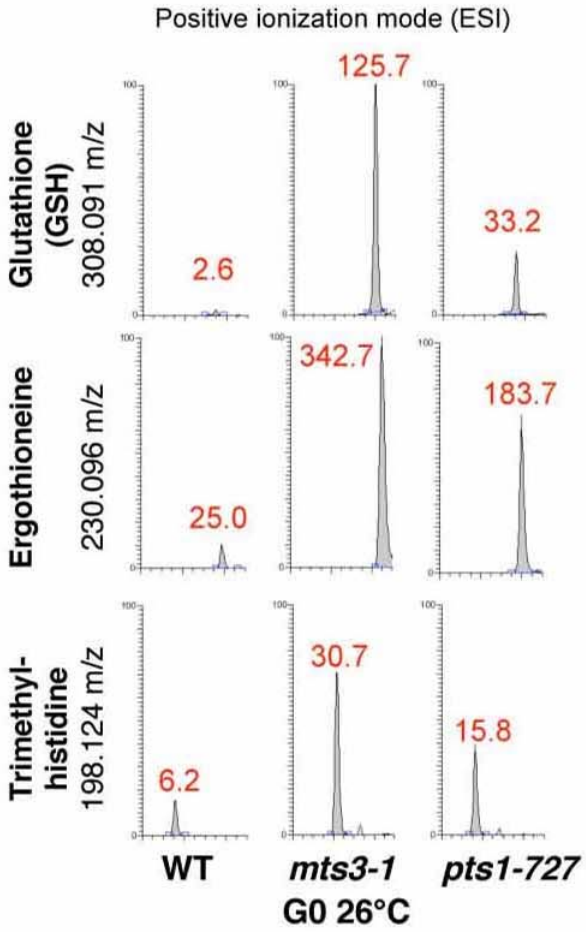
Positive ionization mode (ESI)
Glutathione (GSH)
308.091 m/z
125.7
33.2
2.6
Ergothioneine
230.096 m/z
342.7
183.7
25.0
Trimethyl-histidine
198.124 m/z
30.7
15.8
6.2
WT
mts3-1
pts1-727
G0 26°C

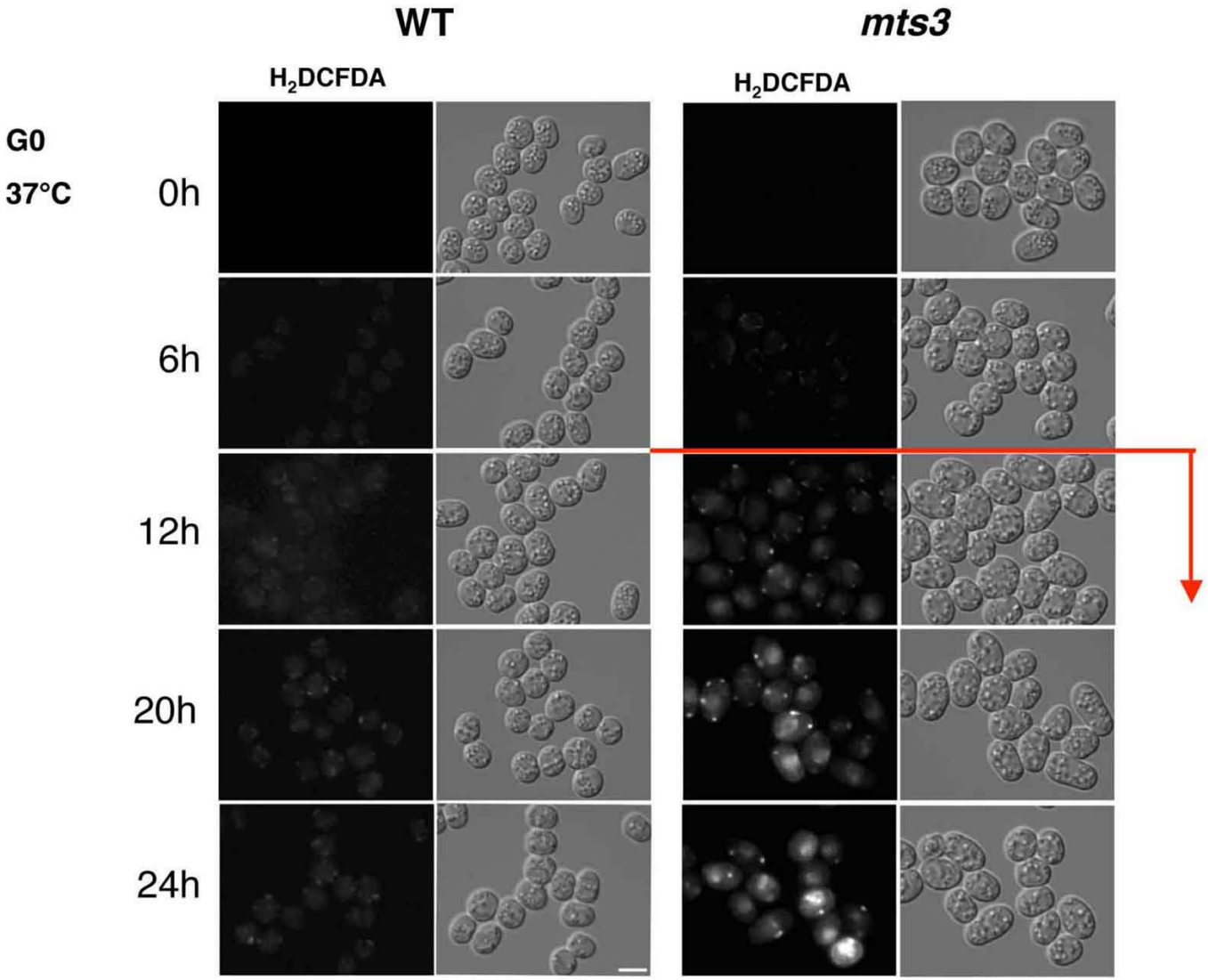
WT
mts3
H2DCFDA
H2DCFDA
G0
37°C
0h
6h
12h
20h
24h

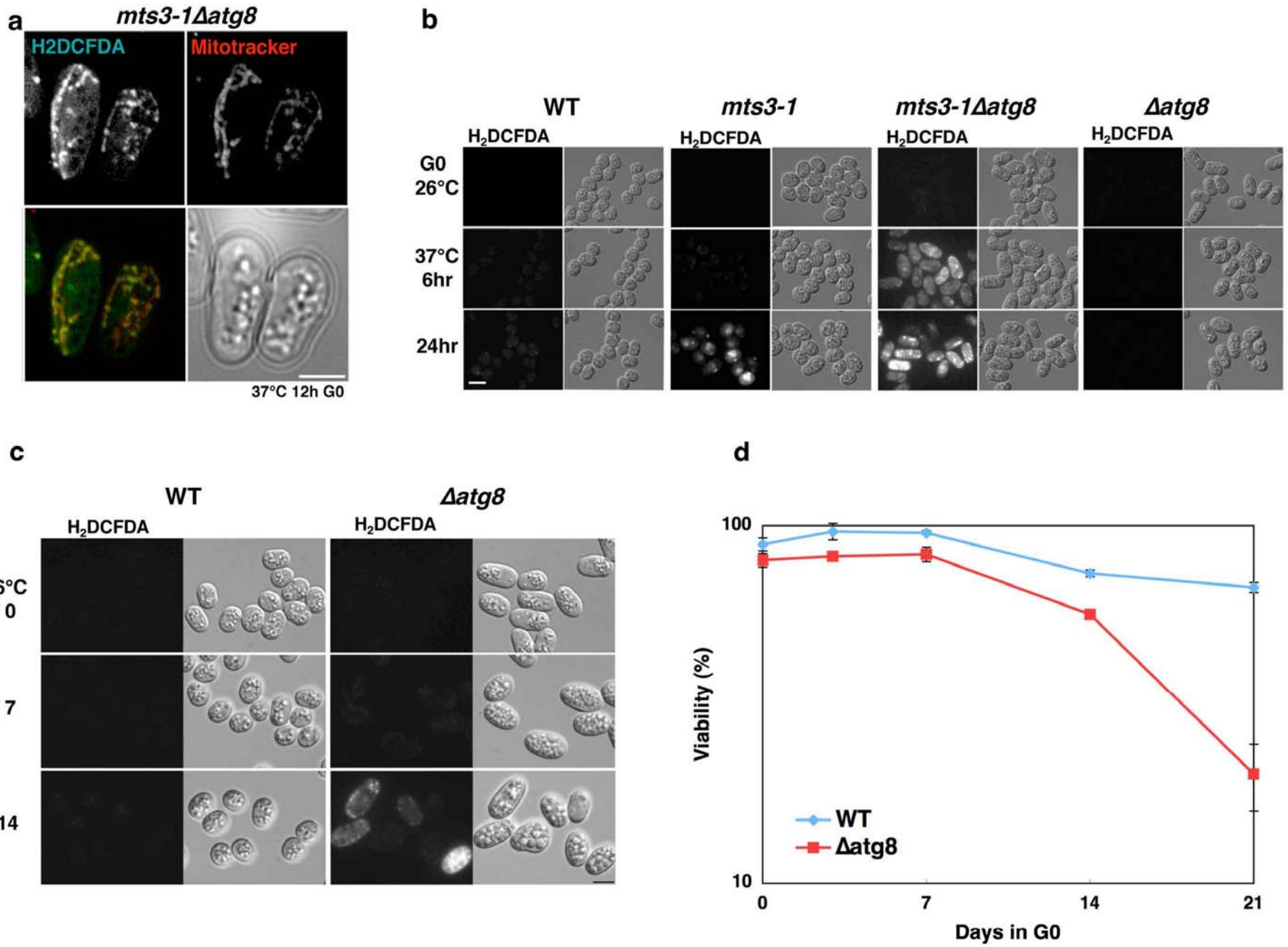
a
mts3-1Δatg8
H2DCFDA
Mitotracker
37°C 12h G0
b
WT
mts3-1
mts3-1Δatg8
Δatg8
H2DCFDA
G0 26°C
37°C 6hr
24hr
c
WT
Δatg8
H2DCFDA
G0 26°C Day 0
Day 7
Day14
d
Viability (%)
100
10
0
7
14
21
Days in G0
WT
Δatg8

rank	Systematic name	Gene product	ratio (mts3/WT)
1	SPAC140.01	sdh2, succinate dehydrogenase (ubiquinone) iron-sulfur protein subunit	0.017237734
2	SPCC191.07	cyc1, cytochrome c	0.021365018
3	SPBC56F2.12	ilv5, acetohydroxyacid reductoisomerase	0.034667114
4	SPBC1861.05	carbohydrate kinase	0.038058156
5	SPCC1682.09c	guanine nucleotide transporter	0.040352681
6	SPAC2E1P3.04	copper amine oxidase	0.046434356
7	SPAC31G5.14	gcv1/n313, glycine decarboxylase T subunit	0.052590401
8	SPAC17G8.06c	dihydroxy-acid dehydratase	0.056145702
9	SPAC4G9.10	arg3, ornithine carbamoyltransferase Arg3	0.069272546
10	SPAC31G5.13	rpn11/pad1/sks1/bfr2/mts5, 19S proteasome regulatory subunit Rpn11	0.076104234
11	SPBC24C6.06	gpa1, G-protein alpha subunit	0.077219007
12	SPAC343.16	lys2, homoaconitate hydratase Lys2	0.079472592
13	SPBC776.07	conserved eukaryotic protein	0.08135805
14	SPAC20G8.04c	electron transfer flavoprotein-ubiquinone oxidoreductase	0.083210352
15	SPBC3H7.03c	2-oxoglutarate dehydrogenase (lipoamide) (e1 component of oxoglutarate dehydrogenase complex)	0.083928498
16	SPBP4H10.08	qcr10, ubiquinol-cytochrome-c reductase complex subunit Qcr10	0.085743094
17	SPBC13E7.04	atp16, F1-ATPase delta subunit	0.086856339
18	SPAC23H4.06	gln1, glutamate-ammonia ligase Gln1	0.099162728
19	SPBC3B8.04c	membrane transporter	0.101333065
20	SPBC9B6.04c	tuf1, mitochondrial translation elongation factor EF-Tu Tuf1	0.104605855
21	SPBC16E9.05	erg6, delta-sterol C-methyltransferase	0.106877342
22	SPBC215.08c	arg4, carbamoyl-phosphate synthase Arg4	0.109039557
23	SPBC25H2.09	conserved fungal protein	0.109446095
24	SPBC428.02c	eca39, branched chain amino acid aminotransferase Eca49	0.110259506
25	SPBP4H10.15	aconitate hydratase	0.111028725
26	SPAC5D6.04	auxin family	0.112204073
27	SPCC794.01c	glucose-6-phosphate 1-dehydrogenase	0.113196268
28	SPAC17G6.06	rps2401/rps24-1/rps24, 40S ribosomal protein S24	0.115663736
29	SPAC694.04c	conserved eukaryotic protein	0.116555091
30	SPCC1223.09	uricase	0.117571321

31	SPAC589.12	cell wall organization membrane protein	0.118220669
32	SPBPB7E8.02	conserved protein (fungal bacterial protazoan)	0.122633948
33	SPBC83.05	RNA-binding protein	0.126252093
34	SPAC1002.09c	dld1/dldh, dihydrolipoamide dehydrogenase Dld1	0.126321073
35	SPAC6F12.07	tom20, mitochondrial TOM complex subunit Tom20	0.126458608
36	SPCC576.01c	sulfonate dioxygenase	0.130972881
37	SPCC1919.12c	aminopeptidase	0.138324598
38	SPBC21B10.03c	ataxin-2 homolog	0.14097368
39	SPBC27B12.14	mitochondrial membrane protein complex assembly protein	0.141042954
40	SPCC1322.16	prohibitin Phb2	0.142201696
41	SPCC663.03	pmd1, leptomycin efflux transporter	0.143489968
42	SPAC13G6.06c	glycine cleavage complex subunit P	0.147050306
43	SPCC70.03c	proline dehydrogenase	0.147890882
44	SPAC24C9.05c	conserved protein (fungal and plant)	0.150779976
45	SPCC1620.08	succinate-CoA ligase (beta subunit)	0.151870563
46	SPAC16E8.17c	succinate-CoA ligase (alpha subunit)	0.152341997
47	SPAC19A8.04	erg5, C-22 sterol desaturase Erg5	0.152812397
48	SPBP23A10.10	ppk32, serine/threonine protein kinase Ppk32	0.153989165
49	SPAC6G10.08	idp1, isocitrate dehydrogenase Idp1	0.154369903
50	SPAC1296.02	cox4, cytochrome c oxidase subunit IV	0.155525086
51	SPMIT.09	atp8, F0-ATPase subunit 8	0.158507042
52	SPCC18.18c	fum1, fumarate hydratase	0.161325045
53	SPAC1B2.05	mcm5/nda4, MCM complex subunit Mcm5	0.161533452
54	SPBC56F2.09c	arg5, arginine specific carbamoyl-phosphate synthase Arg5	0.162527774
55	SPAC1782.07	qcr8, ubiquinol-cytochrome-c reductase complex subunit 7	0.165691978
56	SPBC27B12.13	tom40, mitochondrial TOM complex subunit Tom40	0.168994063
57	SPAPYUK71.03c	C2 domain protein	0.173651985
58	SPAC22E12.14c	sck2, serine/threonine protein kinase Sck2	0.175440883
59	SPCC1235.15	dga1, diacylglycerol O-acyltransferase	0.177259585
60	SPBC14C8.04	acetolactate synthase regulatory unit	0.184095184
61	SPAC27D7.06	electron transfer flavoprotein alpha subunit	0.184113308
62	SPCC1223.08c	dfr1, dihydrofolate reductase Dfr1	0.186668209

63	SPCC74.02c	mRNA cleavage and polyadenylation specificity factor complex associated protein	0.189513758
64	SPBC146.09c	lsd1, histone demethylase	0.189788877
65	SPAC18B11.11	GTPase activating protein	0.193179682
66	SPCC132.04c	NAD-dependent glutamate dehydrogenase	0.193278887
67	SPCC70.02c	ATPase inhibitor	0.193431581
68	SPAC6C3.04	cit1, citrate synthase	0.194366523
69	SPMIT.11	cox2, cytochrome c oxidase 2	0.194616826
70	SPBC725.10	tspO homolog	0.195625537
71	SPAC1A6.10	Moeb/ThiF domain	0.197001786
72	SPAC14C4.04	B22918-2, hypothetical protein	0.198955801
73	SPAC1039.06	alanine racemase	0.199519859
74	SPBC3E7.16c	leu3, 2-isopropylmalate synthase	0.200632445
75	SPBC1289.09	tim21, mitochondrial inner membrane presequence translocase complex subunit Tim21	0.201715544
76	SPBC947.15c	NADH dehydrogenase	0.202609506
77	SPACUNK4.15	2',3'-cyclic-nucleotide 3'-phosphodiesterase	0.203525557
78	SPAC19B12.04	SPAC19B12.04/rps3001/rps30-1,SPBC19G7.03c/rps3002/rps30-2/rps30, 40S ribosomal protein S30	0.205601776
79	SPBP35G2.07	ilv1, acetolactate synthase catalytic subunit	0.205731272
80	SPAC24C9.06c	aconitate hydratase	0.206965878
81	SPCC320.14	threo-3-hydroxyaspartate ammonia-lyase	0.209106776
82	SPBC31F10.15c	atp15, F0-ATPase epsilon subunit	0.209248865
83	SPAC15E1.03	rpl36a, 60S ribosomal protein L36/L42	0.209248865
84	SPAC1556.02c	sdh1, succinate dehydrogenase Sdh1	0.209863604
85	SPAC823.05c	tlg2, SNARE Tlg2	0.210500694
86	SPBC29A10.01	ccr1, NADPH-cytochrome p450 reductase	0.210786389
87	SPAC869.04	formamidase-like protein	0.21208836
88	SPAC521.03	short chain dehydrogenase	0.212791872
89	SPBP16F5.08c	flavin dependent monooxygenase	0.21302043
90	SPCC830.11c	adenylate kinase	0.213706308
91	SPAC17H9.16	tom22, mitochondrial TOM complex subunit Tom22	0.214268277
92	SPBC29B5.02c	isp4, OPT oligopeptide transporter family	0.215817295
93	SPBC17G9.07	rps2402/rps24-2, 40S ribosomal protein S24	0.217652858
94	SPBC725.02	mpr1/spy1, speedy homolog	0.219292207

95	SPBC530.10c	anc1, adenine nucleotide carrier Anc1	0.219592837
96	SPAC31G5.04	homoisocitrate dehydrogenase	0.220421608
97	SPAC23C11.13c	hpt1, xanthine phosphoribosyltransferase	0.222862044
98	SPCC1450.15	pig-F	0.224407798
99	SPAC23C11.11	cka1/orb5, serine/threonine protein kinase Cka1	0.224995993
100	SPBC1215.01	shy1, SURF-family protein Shy1	0.225835439
101	SPBC725.01	aspartate aminotransferase	0.227935626
102	SPBC31F10.07	cortical component Lsb5	0.229705478
103	SPCC18B5.11c	cds1, replication checkpoint kinase Cds1	0.231507884
104	SPAC644.09	alanine racemase	0.23204236
105	SPAC1F12.02c	p23fy, translationally controlled tumor protein homolog	0.233152409
106	SPAC23A1.03	apt1, adenine phosphoribosyltransferase (APRT)	0.233215492
107	SPAC12G12.04	mcp60/hsp60, heat shock protein Hsp60	0.234108739
108	SPBC409.10	ade7, phosphoribosylamidoimidazolesuccinocarboxamide synthase Ade7	0.234172146
109	SPAC823.15	ppa1, minor serine/threonine protein phosphatase Ppa1	0.234837347
110	SPCC1259.09c	pyruvate dehydrogenase protein x component	0.236374437
111	SPBP8B7.05c	carbonic anhydrase	0.23815151
112	SPAC4G9.04c	cleavage and polyadenylation specificity factor	0.238937026
113	SPAC19A8.05c	vps27, sorting receptor for ubiquitinated membrane proteins	0.239026252
114	SPAC9E9.03	leu2, 3-isopropylmalate dehydratase Leu2	0.239030452
115	SPCP1E11.02	ppk38, Ark1/Prk1 family protein kinase Ppk38	0.239428039
116	SPAC343.17c	WD repeat protein, human WDR70 family	0.240410695
117	SPBC25B2.06c	btb2, BTB/POZ domain protein Btb2	0.241752986
118	SPCC1183.11	MS ion channel protein 1	0.24253204
119	SPAC23C4.09c	DNA-binding TFAR19-related protein	0.243202073
120	SPAC6F12.02	rst2, transcription factor Rst2	0.243288058
121	SPBC119.17	metallopeptidase	0.24346154
122	SPAC3A11.07	NADH dehydrogenase	0.243830431
123	SPBC2G2.08	ade9, C-1-tetrahydrofolatesynthase/methylenetetrahydrof olatedehydrogenase/methylenetetrahydrofolatecyclohydrolase/formyltetrahydrofolate synthetase	0.244949255
124	SPAC1002.03c	gls2, glucosidase II Gls2	0.246563074
125	SPAC1A6.07	sequence orphan	0.247279817

rank	Systematic name	Gene product	ratio (mts3/WT)	Cd+2	H2O2
1	SPBC3E7.02c	hsp16, heat shock protein Hsp16	146.8581995	+	–
2	SPCC663.08c	short chain dehydrogenase	62.74615283	–	+
3	SPCC663.06c	short chain dehydrogenase	53.17919385	+	+
4(*)	SPBC83.17	transcriptional coactivator, multiprotein bridging factor Mbf1	33.34068723	–	–
5	SPAC11D3.01c	conserved fungal protein	28.0201278	+	+
6	SPAC32A11.02c	conserved fungal protein	21.55927065	+	–
7	SPCC757.03c	ThiJ domain protein	20.57226539	+	+
8	SPAC139.05	succinate-semialdehyde dehydrogenase	18.48161055	+	+
9	SPBC1773.05c	tms1, hexitol dehydrogenase	15.83920026	+	+
10	SPAPJ691.02	yippee-like protein	13.9015024	–	+
11	SPAC13A11.06	pyruvate decarboxylase	12.99818471	–	–
12	SPCC1281.07c	glutathione S-transferase Gst3	12.56782373	–	+
13	SPBC887.01	acireductone dioxygenase family	12.34299012	–	–
14	SPACUNK4.17	NAD binding dehydrogenase family protein	12.32845218	+	+
15	SPAC513.06c	dihydrodiol dehydrogenase	12.26436079	–	+
16	SPAC977.16c	dak2, dihydroxyacetone kinase Dak2	12.02308085	+	–
17	SPCC830.07c	psi1/psi, DNAJ domain protein Psi1	11.83455111	+	–
18	SPAC1786.02	phospholipase	11.53960213	–	–
19	SPAC869.02c	nitric oxide dioxygenase	10.07676961	–	+
20	SPAC4F10.09c	ribosome biogenesis protein Noc1	10.02147028	–	–
21	SPBP4H10.07	ubiquitin-protein ligase E3	10.01224113	–	–
22	SPBC12C2.03c	FAD binding protein	9.887646211	–	–
23	SPBC1198.13c	tfg2, transcription factor TFIIF complex beta subunit Tfg2	9.575179452	–	–
24	SPCC417.07c	mto1/mbo1/mod20, MT organizer Mto1	9.566265854	–	–
25	SPBC725.03	conserved fungal protein	9.28405898	+	+
26	SPAC23G3.09	taf4, transcription factor TFIID complex subunit Taf4	9.108389758	–	–
27	SPCC757.12	alpha-amylase homolog	8.8215832	–	–
28	SPAC1687.09	conserved fungal protein	8.357111058	–	–
29	SPCC1223.02	nmt1/thi3, no message in thiamine Nmt1	8.351475911	–	–
30	SPAC23H4.01c	sterol binding ankyrin repeat protein	8.295490382	–	–
31	SPBP4H10.12	conserved protein (fungal and bacterial)	8.132940624	+	–

32	SPBC3B9.01	Hsp70 nucleotide exchange factor	8.036168957	+	−
33	SPAC2C4.15c	ubx2/ucp13, UBX domain protein Ubx2	7.738747368	−	−
34	SPBC115.03	gfo/idh/mocA family oxidoreductase	7.729149701	−	−
35	SPAC1B3.03c	wis2/cyp5, cyclophilin family peptidyl-prolyl cis-trans isomerase Wis2	7.542579362	−	−
36	SPBC2D10.03c	conserved eukaryotic protein	7.483183967	−	−
37	SPAC823.03	ppk15, serine/threonine protein kinase Ppk15	7.458771177	−	−
38	SPCC895.05	for3, formin For3	7.456118631	−	−
39	SPBC119.03	S-adenosylmethionine-dependent methyltransferase	7.3535792	+	+
40	SPAC9G1.10c	inositol polyphosphate phosphatase	7.342028207	−	−
41	SPAC26H5.05	IPT/TIG ankyrin repeat protein	7.240172354	−	−
42	SPCC14G10.02	ribosome biogenesis protein Urb1	7.236706028	−	−
43	SPAC17A5.06	ptr8, transcription factor TFIIH complex ERCC-3 subunit	7.20796805	−	−
44	SPAC9E9.13	wos2, p23 homolog	7.112611911	−	−
45	SPCC18.03	shuttle craft like transcriptional regulator	7.106318617	−	−
46	SPAC5H10.05c	NADHdh_2 domain protein	6.81479964	−	−
47	SPAC23H3.15c	sequence orphan	6.654241946	+	+
48	SPBC23G7.10c	NADH-dependent flavin oxidoreductase	6.598656321	+	+
49	SPAC56F8.02	AMP binding enzyme	6.528217989	−	−
50	SPAC2F7.03c	pom1, DYRK family protein kinase Pom1	6.414216795	−	−
51	SPBC30B4.02c	R3H and G-patch domain, unknown biological role	6.394966186	−	−
52	SPBC19G7.01c	msh2/swi8/mut3, MutS protein homolog 2	6.285064576	−	−
53	SPCC965.07c	gst2, glutathione S-transferase Gst2	6.118014916	+	+
54	SPAP8A3.04c	hsp9/scf1, heat shock protein Hsp9	6.082615309	+	+
55	SPBC15C4.05	ATP-dependent RNA/DNA helicase	6.058637488	−	−
56	SPAC22E12.18	conserved fungal protein	5.906127199	−	−
57	SPBC1539.10	ribosome biogenesis protein Nop16	5.890841874	−	−
58	SPAC2H10.02c	26S proteasome regulator	5.844724218	−	−
59	SPBC11B10.09	cdc2/swo2, cyclin-dependent protein kinase Cdc2	5.653448517	−	−
60	SPBC3H7.07c	phosphoserine phosphatase	5.643085113	−	−
61	SPAC13G7.02c	ssa1, heat shock protein Ssa1	5.609986138	+	+
62	SPAC2F7.16c	phospholipase D	5.496443501	−	−
63	SPBC215.02	bob1/gim5, prefoldin subunit 5	5.457598994	−	−

64	SPCC18.16c	fmn1, riboflavin kinase Fmn1	5.440689734	−	−
65	SPAC20H4.10	ufd2, ubiquitin-protein ligase E4	5.419775645	−	−
66	SPAC4G8.05	ppk14, serine/threonine protein kinase Ppk14	5.350200091	−	−
67	SPBC11C11.08	srp1, SR family protein Srp1	5.309557959	−	−
68	SPAC19D5.05c	U3 snoRNP-associated protein Imp3	5.285843471	−	−
69	SPBC6B1.02	ppk30, Ark1/Prk1 family protein kinase Ppk30	5.225206781	−	−
70	SPBC29A3.02c	his7, phosphoribosyl-AMP cyclohydrolase/phosphoribosyl-ATP pyrophosphohydrolase His7	5.223196042	−	−
71	SPAC23C11.06c	hydrolase	5.216335057	+	+
72	SPCC736.11	ago1/csp9, argonaute	5.203361813	−	−
73	SPBC4F6.07c	ATP-dependent RNA helicase Mak5	5.18123671	−	−
74	SPBC31F10.13c	hip1/hir1, hira protein Hip1	5.179537419	−	−
75	SPCC1682.16	rpt4, 19S proteasome regulatory subunit Rpt4	5.153884228	−	−
76	SPCC736.07c	cell polarity protein	5.124927963	−	−
77	SPBC1105.09	ubc15, ubiquitin conjugating enzyme Ubc15	5.122237328	−	−
78	SPCC188.08c	ubp22/ubp5, ubiquitin C-terminal hydrolase Ubp22	5.081343766	−	−
79	SPAC637.03	conserved fungal protein	5.056896177	+	+
80	SPBC29A10.16c	cytochrome b5	5.038926778	−	−
81	SPBC16E9.16c	sequence orphan	5.032332597	+	+
82	SPAC1F5.03c	FAD-dependent oxidoreductase	5	−	−
83	SPCC10H11.01	prp11, ATP-dependent RNA helicase Prp11	4.95298747	−	−
84	SPAC26H5.04	vacuolar import and degradation protein Vid28	4.929505163	−	−
85	SPAC637.10c	rpn10/pus1, 19S proteasome regulatory subunit Rpn10	4.929139266	−	−
86	SPAC16E8.09	scd1/ral1, RhoGEF Scd1	4.782668255	−	−
87	SPBC4F6.17c	mitochondrial matrix chaperone Hsp78	4.729265028	+	−
88	SPBC887.03c	noc3, Noc2p-Noc3p complex subunit Noc3	4.679266344	−	−
89	SPAC19G12.08	fatty acid hydroxylase	4.654088269	−	−
90	SPAC2F3.05c	xylose and arabinose reductase	4.55290016	+	+
91	SPAC1F12.10c	NADPH-hemoprotein reductase	4.468348315	+	−
92	SPCC4G3.13c	CUE domain protein Cue1/4 family	4.465687769	−	−
93	SPAPB24D3.08c	NADP-dependent oxidoreductase	4.461833822	+	+
94	SPAC3G6.07	sequence orphan	4.408353597	−	+
95	SPAC664.03	RNA polymerase II associated Paf1 complex	4.361076594	−	−

96	SPCC63.08c	ppk36/atg1, serine/threonine protein kinase Ppk36	4.345699119	−	+
97	SPCP1E11.04c	pal1, membrane associated protein Pal1	4.32697659	−	−
98	SPBC16A3.09c	ufd1, Cdc48-Ufd1-Npl4 complex component Ufd1	4.298752047	−	−
99	SPCC1281.06c	acyl-coA desaturase	4.295212156	−	−
100	SPAC26A3.16	dph1/ucp5, UBA domain protein Dph1	4.295086395	−	−
101	SPBC543.04	conserved eukaryotic protein	4.264481805	−	−
102	SPAC806.02c	Par A family ATPase iron cluster assembly protein	4.232380317	−	−
103	SPBC336.04	cdc6/pol3/pold/mis10, DNA polymerase delta catalytic subunit Cdc6	4.223632666	−	−
104	SPBC4B4.01c	pantothenate kinase	4.210589297	−	−
105	SPAC27F1.05c	4-aminobutyrate transaminase	4.208488661	−	−
106	SPBC119.13c	prp31, U4/U6 x U5 tri-snRNP complex subunit Prp31	4.171436572	−	−
107	SPCC1281.04	pyridoxal reductase	4.122035273	+	+
108	SPBC409.13	6,7-dimethyl-8-ribityllumazine synthase	4.120889047	−	+
109	SPAC23H3.02c	ini1, RING finger-like protein Ini1	4.111807053	−	−
110	SPCC1235.14	ght5, hexose transporter Ght5	4.017454955	−	−